1

Transport through the Energy Barriers: Transition Probability

In this chapter electron transport through energy barriers and wells is considered. Based on transfer matrix technique, tunneling probability through different nanostructures, quantum barriers, and quantum wells is described. Tunneling through triangular barrier at electron field emission is considered as a special case. The effects of charge trapping in barrier and temperature effect are also analyzed. Great attention is paid to resonant tunneling of electrons and time parameters of this process.

1.1 Transfer Matrix Technique

In order to describe the electron transport through structure containing energy barriers and wells the matrix method is commonly used [1–3]. The matrix method is based on the continuity of the wave function and its first derivative at any heterostructures (Figure 1.1). It allows determining the incidence energy dependence of transmission probability. Using the envelope wave function under effective mass approximation the wave function of particle with the incident and reflected waves amplitudes of A_n and B_n at any segment n is:

$$\Psi_n(x) = A_n e^{ik_n x} + B_n e^{-ik_n x}. \tag{1.1}$$

with wave vector, k_n

$$k_n = \sqrt{2m'^*_n(E - U_n)/\hbar^2} \tag{1.2}$$

where E is the incident electron energy and U_n is the potential related to the reference n segment (Figure 1.1).

The following matrix equation can be written:

$$\begin{pmatrix} A_{n+1} \\ B_{n+1} \end{pmatrix} = \prod_{p=1}^{n} M_p \begin{pmatrix} A_1 \\ B_1 \end{pmatrix} \tag{1.3}$$

Vacuum Nanoelectronic Devices: Novel Electron Sources and Applications, First Edition.
Anatoliy Evtukh, Hans Hartnagel, Oktay Yilmazoglu, Hidenori Mimura and Dimitris Pavlidis.

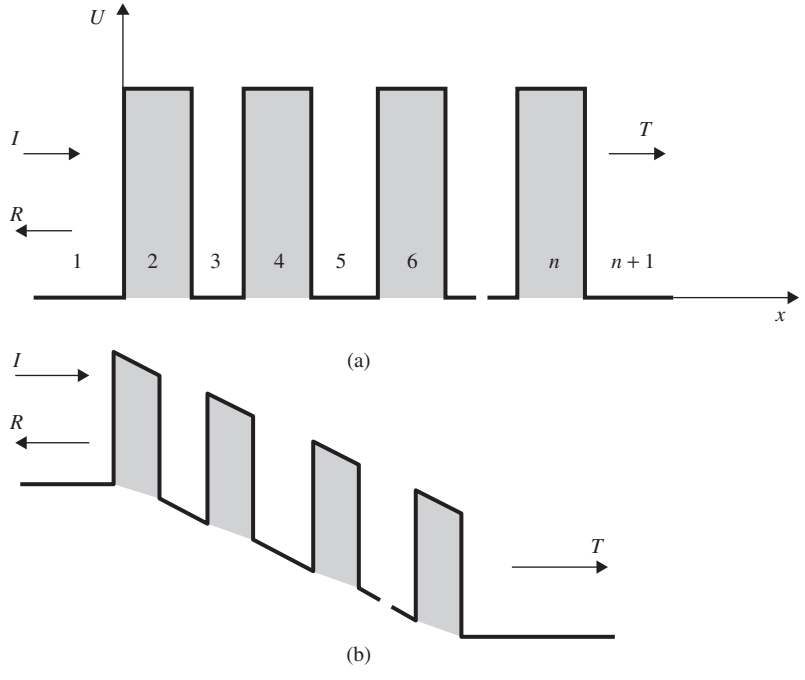

Figure 1.1 Multilayer structure with barriers and wells at (a) zero and (b) applied bias

The matrix M_p is generated by invoking the continuity of the wave function $\Psi(x)$ and its first derivative by properly accounting for the effective mass,

$$\frac{1}{m_n^*}\frac{d\Psi_n}{dx} \tag{1.4}$$

at the interface n. The transmission probability at any energy $T(E)$ is given as

$$T(E) = \frac{m_1^*}{m_{n+1}^*}\frac{k_{n+1}}{k_1}\left|\frac{A_{n+1}}{A_1}\right|^2. \tag{1.5}$$

If we assume $A_1 = 1$

$$T(E) = \frac{m_1^*}{m_{n+1}^*}\frac{k_{n+1}}{k_1}\left|A_{n+1}\right|^2. \tag{1.6}$$

To clarify the idea of transfer matrix technique let's consider one obstacle (potential barrier border) (Figure 1.2). Equation (1.3) for one barrier can be rewritten as

$$\begin{pmatrix} A_2 \\ B_2 \end{pmatrix} = M_1^{(21)}\begin{pmatrix} A_1 \\ B_1 \end{pmatrix} = \begin{pmatrix} M_{11}^{(21)}, M_{12}^{(21)} \\ M_{21}^{(21)}, M_{22}^{(21)} \end{pmatrix}\begin{pmatrix} A_1 \\ B_1 \end{pmatrix} \tag{1.7}$$

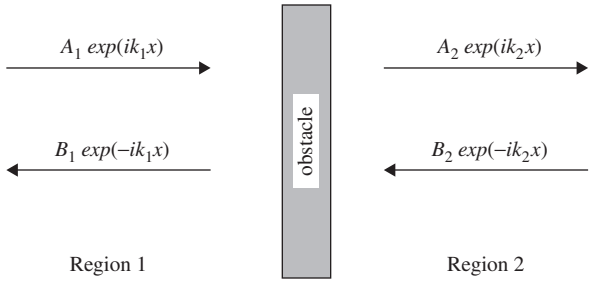

Figure 1.2 Scattering of quantum particle on one obstacle

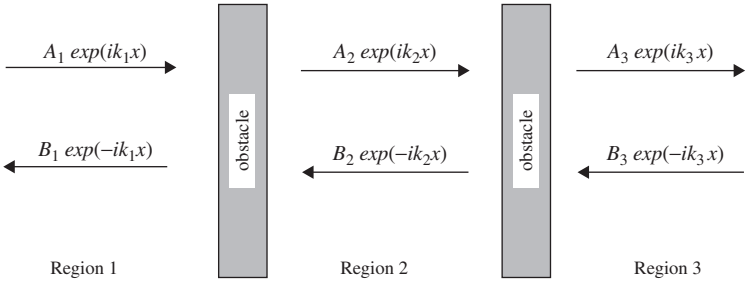

Figure 1.3 Scattering of quantum particle on two obstacles

There are no advantages of transfer matrix technique for scattering process on one barrier. But if we consider a more complicated process of subsequent scattering of particles on two barriers (Figure 1.3), the transfer matrix technique has significant advantages. The amplitudes of particle waves that move from region 1 into region 2 are given by wave amplitudes in region 1 and transfer matrix $M^{(21)}$. The wave amplitudes in region 3, in turn, are connected with wave amplitudes in region 2 by matrix $M^{(32)}$. Accordingly

$$\begin{pmatrix} A_2 \\ B_2 \end{pmatrix} = M_1^{(21)} \begin{pmatrix} A_1 \\ B_1 \end{pmatrix}, \quad \begin{pmatrix} A_3 \\ B_3 \end{pmatrix} = M_2^{(32)} \begin{pmatrix} A_2 \\ B_2 \end{pmatrix} \tag{1.8}$$

Then it is easy to connect wave amplitudes in region 3 with wave amplitudes in region 1:

$$\begin{pmatrix} A_3 \\ B_3 \end{pmatrix} = M_2^{(32)} M_1^{(21)} \begin{pmatrix} A_1 \\ B_1 \end{pmatrix} \equiv M^{(31)} \begin{pmatrix} A_1 \\ B_1 \end{pmatrix}. \tag{1.9}$$

Now it is easy to generalize the method of calculation of transmission coefficient of the quantum particle moving through the multilayer structure. Particle movement in the structure containing n barriers with known transmission coefficient for each of them is shown in Figure 1.4. Sequent consideration of scattering process on each barrier, as in the case of two barrier structure, allows us to write

$$\begin{pmatrix} A_n \\ B_n \end{pmatrix} = M^{(n,n-1)} M^{(n-1,n-2)} \ \ldots \ M^{(32)} M^{(21)} \begin{pmatrix} A_1 \\ B_1 \end{pmatrix} \equiv M^{(n1)} \begin{pmatrix} A_1 \\ B_1 \end{pmatrix}. \tag{1.10}$$

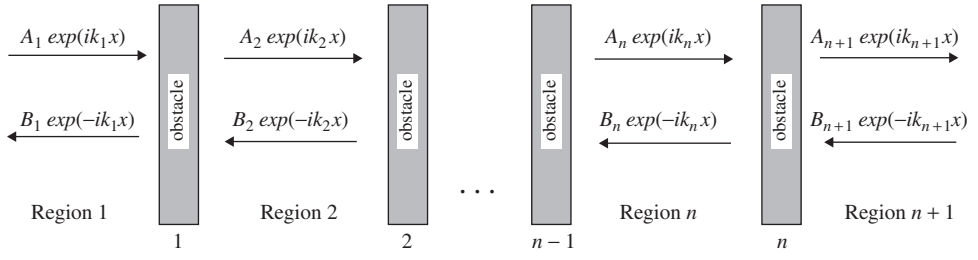

Figure 1.4 Scattering of quantum particle on n obstacles

Thus, to find the amplitudes of waves with n time scattering process, it is necessary simply to find corresponding transfer matrix, which is the product of n matrices for each scattering process.

In this way we obtain the very important result that is the base of transfer matrix technique, namely: transition coefficient in case of n barrier structure is the product of transition matrices of each barrier.

Sometimes instead of $M^{(n,n-1)}$ matrix that connects the wave function amplitudes of the n region from the wave function amplitudes of the $n-1$ region it is useful to use the $M^{(n-1,n)}$ matrix that connects the wave function amplitudes of the $n-1$ region from the wave function amplitudes of the n region. In that case Equation (1.3) can be written:

$$\begin{pmatrix} A_1 \\ B_1 \end{pmatrix} = \prod_{l=1}^{n} M_l' \begin{pmatrix} A_{n+1} \\ B_{n+1} \end{pmatrix} \tag{1.11}$$

$$\begin{pmatrix} A_1 \\ B_1 \end{pmatrix} = M_1' M_2' \ \ldots \ M_n' \begin{pmatrix} A_{n+1} \\ B_{n+1} \end{pmatrix}. \tag{1.12}$$

The reverse matrix for wave amplitude can be obtained by changing the matrices of wave vectors $k_1, k_2, k_3, \ \ldots \ k_n, k_{n+1}$ into $k_{n+1}, k_n, \ \ldots \ k_3, k_2, k_1$, respectively.

The full set of matrices includes the transition through barrier and well regions and borders between regions. In addition to matrices in Equations (1.10) and (1.12) at description of wave function transmission through the heterostructure it is necessary to use the additional matrices which characterize the wave transition inside the barriers and wells. Because of the wave function amplitude of the particle changes only at transition of the barrier border (obstacle) the moving of the particle inside the barrier or well regions causes only the wave function phase shift. The incident wave in point *0* of the barrier has view $A_2 exp(ik_2x)$, and in point d the wave function is $A_2 exp(ik_2x)\ exp(ik_2d)$. This can be represented by diagonal matrix

$$M_1^{(22)} = \begin{pmatrix} M_{11}^{(22)}, M_{12}^{(22)} \\ M_{21}^{(22)}, M_{22}^{(22)} \end{pmatrix} = \begin{pmatrix} e^{ik2d}, 0 \\ 0, e^{-ik2d} \end{pmatrix}, \tag{1.13}$$

and for reverse matrix

$$M_1'^{(22)} = \begin{pmatrix} e^{-ik2d}, 0 \\ 0, e^{ik2d} \end{pmatrix}. \tag{1.14}$$

To demonstrate the transfer matrix method let's consider some simple cases that are the basis for the creation of more complicated multilayer structures. In the following description of the electron transport through barriers and wells we will use reverse matrices.

1.2 Tunneling through the Barriers and Wells

The quantum description of the particle movement through barriers and wells includes the incident wave package, which represents the electron going from the left. This package will go to the barrier and some of them will be reflected, and some will be transmitted. The reflected part of the wave package will give the reflection probability of the electron, and the transmitted part will be the probability of passing on. The package is assumed to be wide, that the incident wave can be represented approximately by the wave function $A_1 exp(ik_1 x)$, where $k_1 = \sqrt{2m_1^* E/\hbar^2} = \frac{2\pi}{\lambda_1}$.

Then the incident wave will give a constant in time density of probability at which the steady flow of electrons will be moving to the right. The average value of the flux density of probability will be $j_0 = (\hbar k_1/m) \times |A_1|^2$. So, despite the presence of flow, to maintain the constant density of probability there must be continuous addition of electrons from the left.

The integral of the normal component of the flux vector on a surface represents the probability that a particle crosses a specified surface in unit time. The flux densities of the incident, reflected, and transmitted particles can be written respectively as

$$j_0 = \frac{\hbar k_1}{m_1^*}\left|A_1\right|^2,\ j_r = \frac{\hbar k_1}{m_1^*}\left|B_1\right|^2,\ j_t = \frac{\hbar k_2}{m_2^*}\left|A_2\right|^2. \tag{1.15}$$

where A_1, B_1, A_2 are the amplitudes of incident, reflected, and transmitted waves respectively, k_1, k_2 are the wave-vectors in regions 1 and 2; and m_1^*, m_2^* are the effective masses of electrons in regions 1 and 2.

For simplicity we assumed $m_1^* = m_2^* = m^*$.

1.2.1 The Particle Moves on the Potential Step

A particle moving toward a finite potential step U_2 at $x = 0$ illustrates the reflection and tunneling effects which are basic features of nanophysics. Suppose $U = 0$ for $x < 0$ and $U = U_2$ for $x > 0$ (Figure 1.5).

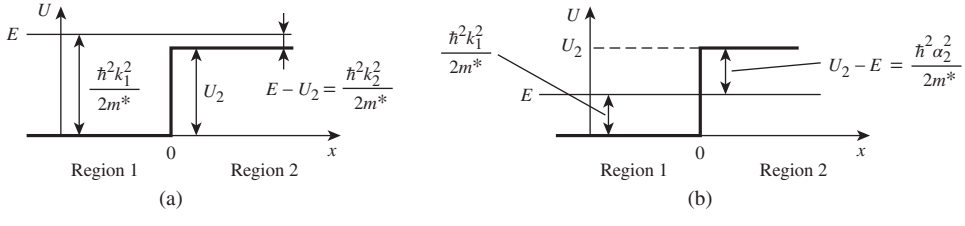

Figure 1.5 The particle moves on the potential step: $E > U_2$ (a) and $E < U_2$ (b)

Let's write a one-dimensional stationary Schrodinger equation for both regions.
For region 1 ($x < 0$)

$$\frac{d^2\Psi_1}{dx^2} + \frac{8\pi^2 m}{h^2} E\Psi_1 = 0, \tag{1.16}$$

for region 2 ($x > 0$)

$$\frac{d^2\Psi_2}{dx^2} + \frac{8\pi^2 m}{h^2}(E - U_2)\Psi_2 = 0, \tag{1.17}$$

where E is the total energy of the electron.

Then wave vectors of the particle moving in region 1 and region 2 are correspondingly

$$k_1 = \sqrt{2m_1^* E/\hbar^2} = \frac{2\pi}{\lambda_1}, \tag{1.18}$$

$$k_2 = \sqrt{2m_2^*(E - U_2)/\hbar^2} = \frac{2\pi}{\lambda_2}, \tag{1.19}$$

where λ_1 and λ_2 are the length of de Broglie waves in regions 1 and 2, respectively.

Using Equations (1.18) and (1.19) Equations (1.16) and (1.17) take the form

$$\frac{d^2\Psi_1}{dx^2} + k_1^2\Psi_1 = 0, \tag{1.20}$$

$$\frac{d^2\Psi_2}{dx^2} + k_2^2\Psi_2 = 0. \tag{1.21}$$

General solutions of these equations can be written as

$$\Psi(x) = \begin{cases} A_1 e^{ik_1 x} + B_1 e^{-ik_1 x}, \ldots\ldots\ldots & x \le 0 \\ A_2 e^{ik_2 x} + B_2 e^{-ik_2 x}, \ldots\ldots\ldots & x \ge 0 \end{cases} \tag{1.22}$$

The wave function of the particle can be considered as two plane waves that move in opposite directions.

Let's consider the features of the electron passing from region 1 to region 2 in two situations: when the total electron energy E is higher than its potential energy U_2 in region 2 (Figure 1.5a) and when $E < U_2$ (Figure 1.5b).

1.2.1.1 Case 1: $E > U_2$

Since the motion of an electron is a plane de Broglie wavelength, then at the regions border 1–2 the wave should be partly reflected and partly penetrated in region 2, or, in other words, moving from one region to another, the electron has a chance to reflect and a chance to go to another region (Figure 1.5a). Determination of these probabilities is the answer to the question about the peculiarities of the electron passing through a potential barrier. Remember that a particular solution to Equation (1.20) $exp(ik_1x)$ characterizes the wave traveling toward the positive axis of X, that is, the incident wave, and the particular solution $exp(-ik_1x)$ corresponds

to the reflected wave. Similar assertions hold for partial solutions $exp(\pm ik_2x)$ Equation (1.22) for the second region ($x > 0$). When $x < 0$ both the incident and reflected waves extend, so we need to consider the general solution of Equation (1.22) where $|A_1|^2$ is the intensity of the incident wave, and $|B_1|^2$ is the intensity of the reflected waves.

The physical constraints on the allowable solutions are essential for solving this problem. First, $B_2 = 0$, since no particles are incident from the right (barrier). Second, at $x = 0$ the required continuity of $\Psi(x)$ implies $A_1 + B_1 = A_2$. Third, at $x = 0$ the derivatives, $d\Psi/dx = A_1 ik_1 exp(ik_1x) - B_1 ik_1 exp(-ik_1x)$ on the left, and $d\Psi/dx = A_2 ik_2 exp(ik_2x)$, on the right, must be equal. Thus

$$A_1 + B_1 = A_2, \tag{1.23}$$

and

$$k_2A_2 = k_1(A_1 - B_1). \tag{1.24}$$

Equations (1.23) and (1.24) are equivalent to

$$B_1 = \frac{k_1 - k_2}{k_1 + k_2}A_1 \text{ and } A_2 = \frac{2k_1}{k_1 + k_2}A_1. \tag{1.25}$$

The reflection and transmission probabilities, R and T, respectively, for the particle flux are then Equation (1.15)

$$R = \frac{k_1|B_1|^2}{k_1|A_1|^2} = \left(\frac{k_1 - k_2}{k_1 + k_2}\right)^2 \tag{1.26}$$

and

$$T = \frac{k_2|A_2|^2}{k_1|A_1|^2} = \frac{4k_1k_2}{(k_1 + k_2)^2}. \tag{1.27}$$

The same results can be obtained with using transfer matrix technique. In this case

$$\begin{pmatrix} A_1 \\ B_1 \end{pmatrix} = M_1^{12} \begin{pmatrix} A_2 \\ B_2 \end{pmatrix}. \tag{1.28}$$

Taking into account the continuity of the wave function and its first derivative at the interface we obtain

$$A_1 + B_1 = A_2 + B_2, \tag{1.29}$$

$$k_1(A_1 - B_1) = k_2(A_2 - B_2). \tag{1.30}$$

We can determine the connection between coefficients that determine the amplitude of wave processes in region 1 (before barrier) and in region 2 (in the barrier).

$$A_1 = \frac{1}{2}\left(1 + \frac{k_2}{k_1}\right)A_2 + \frac{1}{2}\left(1 - \frac{k_2}{k_1}\right)B_2 \tag{1.31}$$

$$B_1 = \frac{1}{2}\left(1 - \frac{k_2}{k_1}\right)A_2 + \frac{1}{2}\left(1 + \frac{k_2}{k_1}\right)B_2 \tag{1.32}$$

and

$$M_1 = \begin{pmatrix} M_{11}, M_{12} \\ M_{21}, M_{22} \end{pmatrix} = \frac{1}{2} \begin{pmatrix} 1 + \frac{k_2}{k_1}, 1 - \frac{k_2}{k_1} \\ 1 - \frac{k_2}{k_1}, 1 + \frac{k_2}{k_1} \end{pmatrix}. \tag{1.33}$$

Taking into account that the particle moves from the left to the right and assume that amplitude of falling wave is equal to 1 ($A_1 = 1$) we obtain for refraction coefficient of wave amplitude

$$r = \frac{B_1}{A_1} = B_1 = \frac{M_{21}}{M_{11}} = \frac{k_1 - k_2}{k_1 + k_2} \tag{1.34}$$

and for transmission coefficient of wave amplitude

$$t = \frac{A_2}{A_1} = A_2 = \frac{1}{M_{11}} = \frac{2k_1}{k_1 + k_2}. \tag{1.35}$$

At this the transmission coefficient for the particles is the ratio of particles that go through the barrier to the particles that fall on the barrier.

$$T = \frac{(\hbar k_2/m^*)}{(\hbar k_1/m^*)}|t|^2 = \frac{4k_1k_2}{(k_1 + k_2)^2}. \tag{1.36}$$

So far as we assumed $m_1^* = m_2^* = m^*$.

The refractive coefficient for the particles is the ratio of particles that reflect from the barrier to the particles that fall on the barrier.

$$R = \frac{(\hbar k_1/m^*)}{(\hbar k_1/m^*)}|r|^2 = \frac{(k_1 - k_2)^2}{(k_1 + k_2)^2}. \tag{1.37}$$

It is easy to see that

$$T + R = 1. \tag{1.38}$$

Substituting in Equations (1.37) and (1.36) the wave vectors of de Broglie wave from Equations (1.18) and (1.19), we determine the reflection R and transmission T coefficients (Figure 1.6) depending on the ratio between the total energy E and potential U_2:

$$R = \left(\frac{1 - \sqrt{1 - \frac{U_2}{E}}}{1 + \sqrt{1 - \frac{U_2}{E}}} \right)^2 \tag{1.39}$$

and

$$T = 4 \frac{\sqrt{1 - \frac{U_2}{E}}}{\left(1 + \sqrt{1 - \frac{U_2}{E}}\right)^2}. \tag{1.40}$$

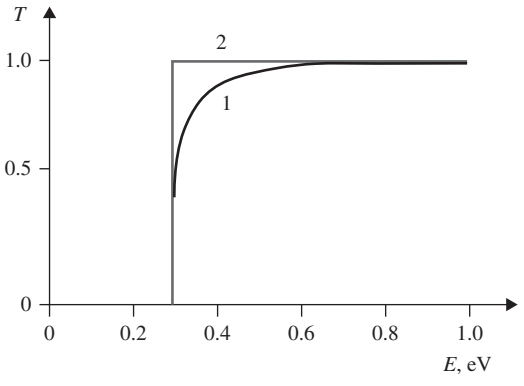

Figure 1.6 Energy dependence of the transmission coefficient of quantum particle (1) at moving over the potential step of 0.3 eV height. Curve 2 is the transmission coefficient in classical case

As can be seen from Equations (1.39) and (1.40), at $E = U_2$ $T = 0$, that is, the particle does not penetrate the barrier. At the electron energy E, twice the barrier, the reflection coefficient has reached quite appreciable value about 3%. These results are very different from the classical ones. In classical mechanics, a particle with energy $E \gg U_2$ always penetrate into the region 2 (at $E = U_2$ kinetic energy E_k is zero). But according to quantum mechanics the particle with $E > U_2$ has finite probability of electron reflection from the barrier.

1.2.1.2 Case 2: $E < U_2$

The only change is that now $E - U_2$ is negative, making k_2 an imaginary number (Figure 1.5b). For this reason k_2 is now written as $k_2 = i\alpha_2$, where

$$k_2 = i\alpha_2 = i\sqrt{2m_2^*(U_2 - E)/\hbar^2}; \tag{1.41}$$

α_2 is a real decay constant. Now the solution for the positive x becomes

$$\Psi(x) = A_2 \ \exp(-\alpha_2 x) + B_2 \ \exp(\alpha_2 x), \tag{1.42}$$

where

$$\alpha_2 = \sqrt{2m_2^*(U_2 - E)/\hbar^2}. \tag{1.43}$$

In this case, $T = 0$, to prevent the particle from unphysical collecting at large positive x. Equations (1.36) and (1.37) and Equation (1.25) remain valid setting $k_2 = i\alpha_2$.

$$T = \frac{(\hbar k_2/m^*)}{(\hbar k_1/m^*)}|t|^2 = \frac{4k_1 i\alpha_2}{(k_1 + i\alpha_2)^2}. \tag{1.44}$$

$$R = \frac{(\hbar k_1/m^*)}{(\hbar k_1/m^*)}|r|^2 = \frac{(k_1 - i\alpha_2)^2}{(k_1 + i\alpha_2)^2}. \tag{1.45}$$

It is seen that $R = 1$, because the numerator and denominator in Equation (1.45) are complex conjugates of each other, and thus have the same absolute value.

Thus, when $E < U_2$ reflection coefficient is 1, that is, the reflection is complete, however, despite the fact that the transmission coefficient $T = 0$, there is a nonzero probability of finding an electron in region 2. The solution for positive x is now an exponentially decaying function, and is not automatically zero in the region of negative energy. In other words, reflection does not occur at the boundary of two regions, while the electrons go at reflection at a certain depth in region 2, then return to the region 1. Indeed, at the imaginary value of k_2 the solution of Schrödinger Equation (1.22) for region 2 becomes

$$\Psi(x) = A_2 \ \exp(ik_2 x) = A_2 \ \exp(-\alpha_2 x), \tag{1.46}$$

and the probability of finding an electron per unit length in region 2 will be

$$\Psi_2 \Psi_2^* = \left|\Psi_2\right|^2 = A_2^2 \ \exp(-2\alpha_2 x). \tag{1.47}$$

Taking into account Equation (1.43) we obtain

$$\left|\Psi_2\right|^2 = A_2^2 \ \exp\left(-\frac{2}{\hbar}\sqrt{2m\left(U_2 - E\right)} \times x\right), \tag{1.48}$$

that is, there is a definite probability of finding the particle in region 2 at a depth of x from the boundary of two regions. However, this probability decreases exponentially with distance from the interface. Thus, when $x = 0.1$ nm and $U_2 - E = 1$ eV the probability of finding an electron is equal to about 0.3, while at $x = 1$ nm the probability is already an order of 10^{-8}. Electron passes into the barrier and turns back, so that the total flux of particles in region 2 is zero. From the wave point of view, this effect is similar to the case of total internal reflection of light, when even at angles greater than critical in the less dense medium is the wave field with exponentially decreasing amplitude, but the flow of energy through the interface over a sufficiently long period of time is equal to zero.

We can determine $|A_2|^2$ from Equation (1.35) assuming $A_1 = 1$, setting $k_2 = i\alpha_2$, and forming $|A_2|^2 = A_2 A_2{}^*$. It is the probability to find the particle at interface ($x = 0$).

$$\left|A_2\right|^2 = \frac{4k_1^2}{(k_1^2 + \alpha_2^2)} = \frac{4E}{U_2}, \tag{1.49}$$

where $E = (\hbar^2 k_1{}^2/2\,m) < U_2$. Note that $|A_2|^2 = 0$ for an infinite potential. Also, this expression agrees in the limit $E = U_2$ with Equation (1.35).

Thus, the probability of finding the particle in the forbidden region of positive x is

$$P(x > 0) = \frac{4E}{U_2}\int_0^\infty \exp(-2\alpha_2 x)dx = \frac{4E}{U_2}\int_0^\infty \exp\left(-\frac{2}{\hbar}\sqrt{2m\left(U_2 - E\right)} \times x\right)dx = \frac{2E}{\alpha_2 U_2}, \tag{1.50}$$

where $E < U_2$.

1.2.2 The Particle Moves above the Potential Barrier

In this case the structure is more complicated because the potential barrier has finite width (Figure 1.7). In contrast to the infinitely wide barrier (potential step), the reflection of electrons will take place both on the border of regions 1 and 2, and on the boundary of regions 2 and 3. Solutions of Schrödinger equations for these regions can be written as

$$\Psi(x) = \begin{cases} A_1 e^{ik_1 x} + B_1 e^{-ik_1 x}, \ldots\ldots\ldots x < x_1 \\ A_2 e^{ik_2 x} + B_2 e^{-ik_2 x}, \ldots\ldots\ldots x_1 < x < x_2 \\ A_3 e^{ik_3 x} + B_3 e^{-ik_3 x}, \ldots\ldots\ldots x > x_2 \end{cases}. \tag{1.51}$$

The particle has energy $E > U_2$. Then wave vectors of particle in region 1, region 2, and region 3 are correspondingly

$$k_1 = \sqrt{2m_1^* E/\hbar^2} \tag{1.52}$$

$$k_2 = \sqrt{2m_2^*(E - U_2)/\hbar^2} \tag{1.53}$$

$$k_3 = \sqrt{2m_1^* E/\hbar^2}. \tag{1.54}$$

To determine the reflection R and transmission T coefficients, we must first find the waves amplitudes A_j and B_j. For this we use the boundary conditions: continuity of Ψ function and its derivative at the boundaries of regions 1–2 and 2–3, that is, at $x = x_1 = 0$ and $x = x_2 = L$. These conditions can be written as

$$(\Psi_1)_{x=0} = (\Psi_2)_{x=0}, \quad \left(\frac{d\Psi_1}{dx}\right)_{x=0} = \left(\frac{d\Psi_2}{dx}\right)_{x=0}, \tag{1.55}$$

$$(\Psi_2)_{x=L} = (\Psi_3)_{x=L}, \left(\frac{d\Psi_2}{dx}\right)_{x=L} = \left(\frac{d\Psi_3}{dx}\right)_{x=L}. \tag{1.56}$$

Solving the system Equations (1.55) and (1.56), we can find an expression for the A_3 because it determines the transmittance T (at $A_1 = 1$):

$$A_3 = \frac{4k_1 k_2 e^{ik_1 d}}{(k_2 + k_1)^2 e^{-ik_2 d} - (k_2 - k_1)^2 e^{ik_2 d}}. \tag{1.57}$$

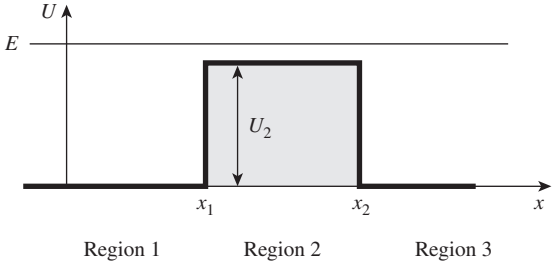

Figure 1.7 The particle moves above the potential barrier

Transmission coefficient is equal to

$$T = \frac{k_3 |A_3|^2}{k_1 |A_1|^2} = |A_3|^2 = A_3 A_3^*, \tag{1.58}$$

where $k_1 = k_3$.

Transfer matrix method simplifies the procedure. In this case

$$\begin{pmatrix} A_1 \\ B_1 \end{pmatrix} = M_1 M_2 M_3 \begin{pmatrix} A_3 \\ B_3 \end{pmatrix} \tag{1.59}$$

where matrix M_1 describes the transition of the border 1–2 from region 2 to region 1 (point x_1)

$$M_1 = \begin{pmatrix} M_{11}, M_{12} \\ M_{21}, M_{22} \end{pmatrix} = \frac{1}{2} \begin{pmatrix} 1 + \frac{k_2}{k_1}, 1 - \frac{k_2}{k_1} \\ 1 - \frac{k_2}{k_1}, 1 + \frac{k_2}{k_1} \end{pmatrix}. \tag{1.60}$$

Diagonal matrix M_2 describes the phase changing of Ψ_2 during the transition of region 2 (barrier).

$$M_2 = \begin{pmatrix} e^{-ik_2 d}, 0 \\ 0, e^{ik_2 d} \end{pmatrix} \tag{1.61}$$

and M_3 describes the transition of the border 2–3 from region 3 to region 2 (point x_2)

$$M_3 = \frac{1}{2} \begin{pmatrix} 1 + \frac{k_3}{k_2}, 1 - \frac{k_3}{k_2} \\ 1 - \frac{k_3}{k_2}, 1 + \frac{k_3}{k_2} \end{pmatrix}. \tag{1.62}$$

Multiplication of the matrices gives such expression for the final matrix

$$\begin{aligned} M &= \begin{pmatrix} M_{11}^{(13)}, M_{12}^{(13)} \\ M_{21}^{(13)}, M_{22}^{(13)} \end{pmatrix} \\ &= \frac{1}{4k_1 k_2} \begin{pmatrix} (k_2 + k_1)^2 e^{-ik_2 d} - (k_2 - k_1)^2 e^{ik_2 d}, (k_2^2 - k_1^2) e^{-ik_2 d} - (k_2^2 - k_1^2) e^{ik_2 d} \\ -(k_2^2 - k_1^2) e^{-ik_2 d} + (k_2^2 - k_1^2) e^{ik_2 d}, -(k_2 - k_1)^2 e^{-ik_2 d} + (k_2 + k_1)^2 e^{ik_2 d} \end{pmatrix} \end{aligned} \tag{1.63}$$

We assume $k_1 = k_3$. According to Equations (1.35) and (1.36) the transmission coefficient can be represented as

$$T = \frac{1}{|M_{11}|^2} = \left| \frac{4k_1 k_2}{(k_2 + k_1)^2 e^{-ik_2 d} - (k_2 - k_1)^2 e^{ik_2 d}} \right|^2 \tag{1.64}$$

It is possible to write the final result as

$$T = \left(1 + \frac{\left(k_2^2 - k_1^2\right)^2}{4k_1^2k_2^2}\sin^2 k_2 d\right)^{-1} \tag{1.65}$$

Note that for integer values of k_2d/π the transmission coefficient, as can be seen from Equation (1.65), equals to 1, that is, the above barrier reflection of the particle is absent.

In this case, twice the length of the potential barrier fits the de Broglie wavelength of the particle $\lambda = 2\pi/k_2$ an integer number of times. These waves cancel each other. At given particle energy the transmission coefficient T as the function of barrier thickness d changes periodically from $T_{min} = 4{k_1}^2{k_2}^2/({k_1}^2 + {k_2}^2)^2$ to $T_{max} = 1$ with a period of $\lambda/2$.

In this case the refractive coefficient R is equal to

$$R = \left(\frac{M_{21}}{M_{11}}\right)^2 = \left|\frac{-\left(k_2^2 - k_1^2\right)e^{-ik_2d} + (k_2^2 - k_1^2)e^{ik_2d}}{(k_2 + k_1)^2e^{-ik_2d} - (k_2 - k_1)^2e^{ik_2d}}\right|^2 \tag{1.66}$$

and

$$T + R = 1 \tag{1.67}$$

We rewrite the Equations (1.65) and (1.66) the using the Equations (1.52)–(1.54) in energy view.

The transmission coefficient is equal to

$$T = \left(1 + \frac{U_2^2}{4E\left(E - U_2\right)}\sin^2 k_2 d\right)^{-1}, \tag{1.68}$$

and the reflection coefficient

$$R = 1 - T = \left(1 + \frac{4E\left(E - U_2\right)}{U_2^2\sin^2 k_2 d}\right)^{-1}. \tag{1.69}$$

Equations (1.68) and (1.69) show that at $T = T_{min}$ the reflection coefficient is $R = R_{max}$.

The most interesting consequence of Equations (1.68) and (1.69) is the appearance of oscillations of transmission and reflection coefficients in dependence on the electron energy E. The oscillation period corresponds to the condition

$$\sin^2(k_2d) = 0 \;\text{ or }\; k_2d = n\pi, \tag{1.70}$$

where $n = 1, 2, 3$, and so on.

At this condition the transmission coefficient of an electron with the wave vector k_2 is $T = 1$, and the reflection coefficient $R = 0$. In this case the integer of half de Broglie wave is placed on the barrier width d for electrons with the wave vector k_2, or with a given energy $E_n = E - U_2$. Indeed, substituting $k_2 = 2\pi/\lambda_2$ in Equation (1.70) we have

$$\frac{2\pi}{\lambda_2}d = n\pi, \;\text{ or }\; d = n\frac{\lambda_2}{2}. \tag{1.71}$$

Semiclassically, this can be interpreted as the result of interference of waves reflected from the boundaries of the barrier, and the incident waves. The last expression can be used to determine the electron energy above the potential barrier

$$E_n = E - U_2 = \frac{mv^2}{2} = \frac{h^2}{2m\lambda_2^2}, \tag{1.72}$$

where $\lambda_2 = h/mv$. Substituting the λ from Equation (1.71), we have

$$E_n = \frac{n^2h^2}{8md^2}. \tag{1.73}$$

The energy E_n, over the barrier coincides with the energy n-th level of an electron localized inside the potential well of width d with infinitely high walls [1].

During the change of electron energy the transmission coefficient oscillates and the maximum value of T_{max} (resonant values) occurs at the condition (1.70). The minimum values of transmittance T_{min} and the corresponding values of energy $E_n' = E' - U_2$, called antiresonant, can be estimated from the condition

$$\sin^2(k_2 d) = 1. \tag{1.74}$$

Hence

$$T_{\min} = \left(1 + \frac{U_2^2}{4E'\left(E' - U_2\right)}\right)^{-1}, \tag{1.75}$$

and

$$E_n' = \frac{h^2}{8md^2}\left(n + \frac{1}{2}\right)^2, \tag{1.76}$$

here $n = 1, 2, 3$, and so on.

With increasing the resonance number n and decreasing the barrier width d the minimum transmission coefficient T_{min} increases rapidly, so that the oscillations are smoothed out. Increasing the barrier height U_2, in contrast, reduces the transmission coefficient, increasing the amplitude of the oscillation [5]. The transmission coefficient of electrons above the potential barrier on their energy dependences at different values of n is shown in Figure 1.8.

It is quite difficult to observe the quantum oscillations of the above barrier electron transmission probability in semiconductor structures experimentally because the oscillation amplitude decreases rapidly with the increasing of the energy, while at low energies the oscillations become blurred due to thermal fluctuations.

1.2.3 The Particle Moves above the Well

In this case the particle also has energy $E > U_2$ (Figure 1.9). Then wave vectors of particle in region 1, region 2, and region 3 are correspondingly

$$k_1 = \sqrt{2m_1^* E/\hbar^2} \tag{1.77}$$

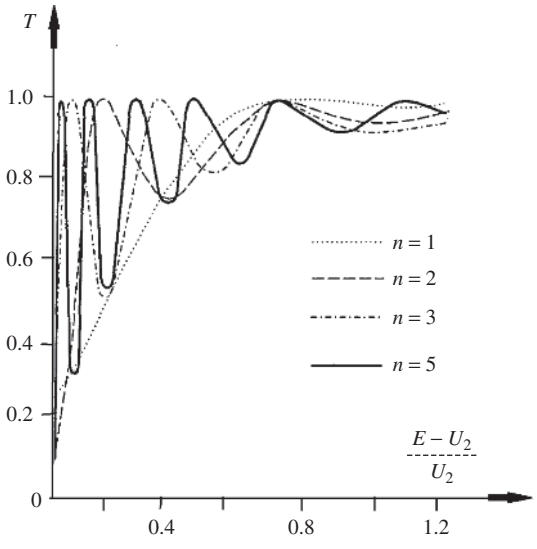

Figure 1.8 Transmission coefficient on energy dependences at moving of the particle above the barrier at $n = 1, 2, 3, 5$

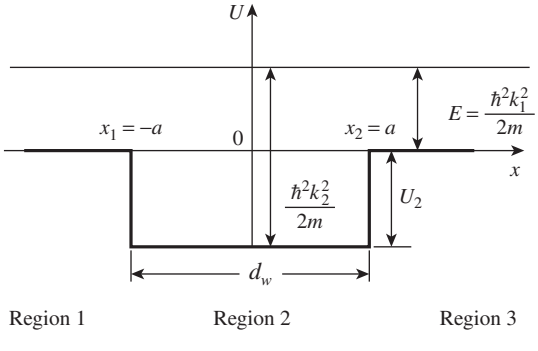

Figure 1.9 The particle moves above the well

$$k_2 = \sqrt{2m_2^*(E + U_2)/\hbar^2} \tag{1.78}$$

$$k_3 = \sqrt{2m_1^* E/\hbar^2}, \tag{1.79}$$

where E is the particle energy, U_2 is the depth of potential well (with the thickness $d_w = 2a$).

Using the procedure described in Section 1.2.2 we obtain

$$T = \left(1 + \frac{(k_2 - k_1)^2}{4k_1^2 k_2^2}\sin^2 k_2 d_w\right)^{-1} \tag{1.80}$$

At integer values of $k_2 d_w/\pi$ the transmission coefficient becomes equal to 1.

The refractive coefficient is

$$R = 1 - T.$$

The transmission coefficient in this case Equation (1.80) is described by the same formulas as in case movement over the barrier Equations (1.65) and (1.68) by replacing U_2 on $-U_2$. As in the case of the potential barrier, as well as in the case of the potential well the oscillations of T have the same nature, namely, semiclassical oscillations can be interpreted as the result of interference of electron waves reflected from the potential jumps at the boundaries of the barrier or well. However, there is a noticeable difference. For equal values of thickness, d, for the barrier and width, d_w, for the well and the same potential energy $|U_2|$ the scale of oscillations of T in the case of passage of the electrons above the barrier are significantly higher than during the passage above the well.

It is possible to find wave functions for such structure in all regions Figure 1.10 [5].

As can be seen the wave function amplitude in region 2 (well) is significantly smaller. It means that at small particle energy $E = \hbar^2 k^2/2m \ll U_2$ the density of probability to find the particle in the well region is significantly lower than outside.

It is more accessible to observe the oscillations of the transmission coefficient at an electron moving above the potential well than at moving above the barrier on experiment, since in this case it is possible to use electrons with relatively small energy.

1.2.4 The Particle Moves through the Potential Barrier

In this case (Figure 1.11) at $E < U_2$ the wave function are

$$\Psi(x) = \begin{cases} A_1 e^{ik_1 x} + B_1 e^{-ik_1 x}, \ldots\ldots\ldots\ x \le x_1 \\ A_2 e^{-a_2 x} + B_2 e^{a_2 x}, \ldots\ldots\ldots\ x_1 \le x \le x_2 \\ A_3 e^{ik_2 x} + B_3 e^{-ik_2 x}, \ldots\ldots\ldots\ x \ge x_2 \end{cases} \tag{1.81}$$

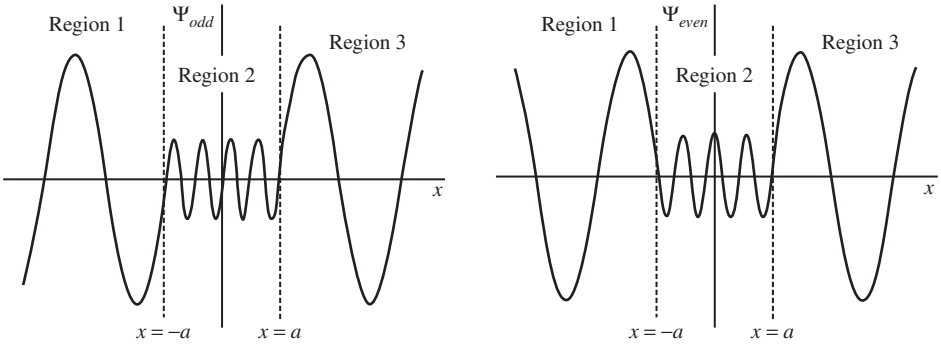

Figure 1.10 The waves of the particle moving above the well

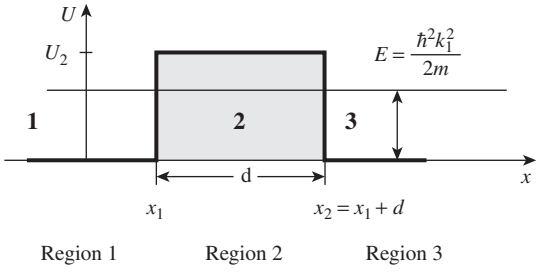

Figure 1.11 The particle moves through the potential barrier

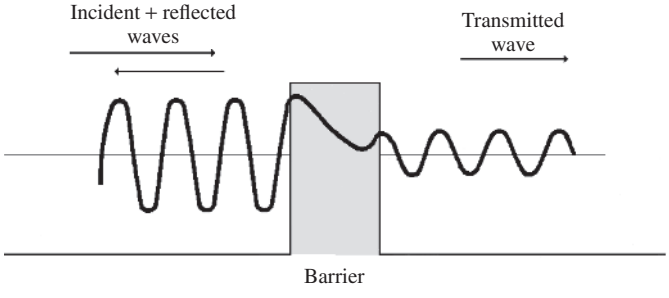

Figure 1.12 Transition of electron waves through the barrier

Then wave vectors of particle movement in region 1, region 2, and region 3 are, respectively:

$$k_1 = \sqrt{2m_1^* E/\hbar^2} \tag{1.82}$$

$$k_2 = i\alpha_2 = i\sqrt{2m_2^*(U_2 - E)/\hbar^2} \tag{1.83}$$

$$k_3 = \sqrt{2m_1^* E/\hbar^2}. \tag{1.84}$$

The schematic image of electron waves at transition through the potential barrier is shown in Figure 1.12.

The procedure for obtaining the transmission coefficient is as in Section 1.2.2 according to Equations (1.59)–(1.63), but in this case we used $k_2 = i\alpha_2$.

As a result the transmission probability is

$$T = \frac{1}{|M_{11}|^2} = \frac{16\alpha_2^2 k_1^2}{[(\alpha_2 + ik_1)^2 e^{-\alpha_2 d} - (\alpha_2 - ik_1)^2 e^{\alpha_2 d}]^2} \tag{1.85}$$

After additional transformation where we take into account that

$$\sinh(x) = \frac{1}{2}[\exp(x) - \exp(-x)], \quad \cosh(x) = \frac{1}{2}[\exp(x) + \exp(-x)], \tag{1.86}$$

$$\cosh^2(x) - \sinh^2(x) = 1, \tag{1.87}$$

we obtain

$$T = \left(1 + \frac{\left(\alpha_2^2 + k_1^2\right)^2}{4k_1^2\alpha_2^2}\sinh^2\alpha_2 d\right)^{-1} \tag{1.88}$$

The penetration of the particle with energy E through the potential barrier U at condition $E < U$ is the well-known tunnel effect. Electron transport through the potential barrier is not associated with the loss of electron energy: the electron leaves the barrier with the same energy with which entry into a barrier. As can be seen from Equation (1.88) in the case of significantly thick and high barrier $\alpha_2 d \gg 1$ the transmission probability T is small enough and exponentially decreases with growth of $\alpha_2 d$ parameter:

$$T = \frac{16k_1^2\alpha_2^2}{(\alpha_2^2 + k_1^2)^2}e^{-2\alpha_2 d}. \tag{1.89}$$

In this case refractive coefficient R is equal to

$$R = \left(\frac{M_{21}}{M_{11}}\right)^2 = \left|\frac{-\left(-a_2^2 - k_1^2\right)e^{\alpha_2 d} + (-\alpha_2^2 - k_1^2)e^{-a_2 d}}{[(\alpha_2 + ik_1)^2 e^{-\alpha_2 d} - (\alpha_2 - ik_1)^2 e^{\alpha_2 d}]^2}\right|^2$$

$$= \left|\frac{\left(a_2^2 + k_1^2\right) \times (e^{\alpha_2 d} - e^{-a_2 d})}{[(\alpha_2 + ik_1)^2 e^{-\alpha_2 d} - (\alpha_2 - ik_1)^2 e^{\alpha_2 d}]^2}\right|^2. \tag{1.90}$$

Formula (1.89) for the transmission coefficient for rectangular barrier can be generalized to the barrier of arbitrary shape (Figure 1.13)

$$T = T_0 \exp\left[-\frac{2\sqrt{2m_2^*}}{\hbar}\int_{x_1}^{x_2}\sqrt{\left(U_2(x) - E\right)}dx\right], \tag{1.91}$$

where T_0 is the constant, order of the unity.

The generalized dependence of transmission probability (through the barrier and above the barrier) on particle energy is shown in Figure 1.14 [6].

In the general case the reverse transfer matrix can be presented as

$$M_p^{(p,p+1)} = \begin{pmatrix} M_{11}^{(p,p+1)}, M_{12}^{(p,p+1)} \\ M_{21}^{(p,p+1)}, M_{22}^{(p,p+1)} \end{pmatrix} = \frac{1}{2}\begin{pmatrix} 1 + \frac{k_{p+1}}{k_p}, 1 - \frac{k_{p+1}}{k_p} \\ 1 - \frac{k_{p+1}}{k_p}, 1 + \frac{k_{p+1}}{k_p} \end{pmatrix}. \tag{1.92}$$

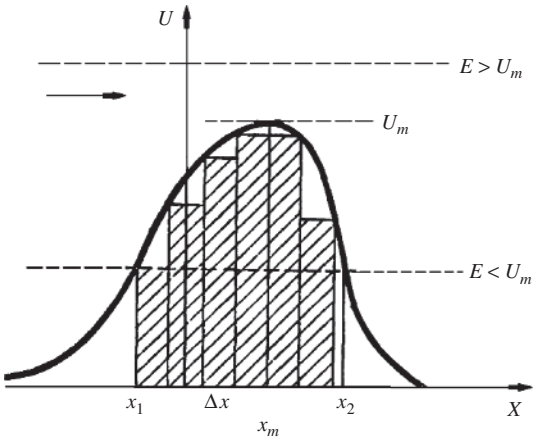

Figure 1.13 Potential barrier of arbitrary shape

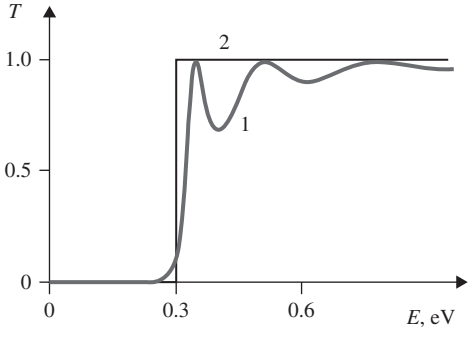

Figure 1.14 Energy dependence of the transmission coefficient of quantum particle (1) at moving through the barrier (AlGaAs) of 0.3 eV height and 10 nm width in GaAs-AlGaAs-GaAs structure. Curve 2 is the transmission coefficient in the classical case

As was summarized in Ref. [7], to describe the transition of the particle through multilayer structure containing barriers and wells based on the transfer matrix technique it is necessary to know four different types of matrices, namely, those respective joint points: within classically allowed regions (M_A), below the barrier (M_B), across discontinuity in the direction from a classically allowed region into the barrier (M_{in}), and across a discontinuity in the direction from the barrier into a classically allowed region (M_{out}).

$$M_A = \begin{pmatrix} e^{-ikw}, 0 \\ 0, e^{ikw} \end{pmatrix}, \tag{1.93}$$

$$M_B = \begin{pmatrix} e^{-\alpha d}, 0 \\ 0, e^{\alpha d} \end{pmatrix}, \tag{1.94}$$

$$M_{in} = \frac{1}{2}\begin{pmatrix} 1 - i\frac{k}{\alpha}, 1 + i\frac{k}{\alpha} \\ 1 + i\frac{k}{\alpha}, 1 - i\frac{k}{\alpha} \end{pmatrix} \tag{1.95}$$

$$M_{out} = \frac{1}{2}\begin{pmatrix} 1 + i\frac{\alpha}{k}, 1 - i\frac{\alpha}{k} \\ 1 - i\frac{\alpha}{k}, 1 + i\frac{\alpha}{k} \end{pmatrix}. \tag{1.96}$$

As can be seen the reverse matrix to M_{in} is M_{out} and vice versa. It was pointed out that the above matrices were particular cases of more general forms which could be derived by exploiting the wave function properties with respect to conjugation and conservation of probability current [3].

In reference [8] the authors approximated the arbitrary potential well by multistep function and then used a matrix method to determine the transmission coefficient. The position dependence of electron effective mass, m_n^*, and permittivity were also approximated by multistep functions. Despite the fact that the matrix method is straightforward, some authors have applied other approaches during the calculation of transmission coefficient. In reference [9] the arbitrary potential well was approximated by piecewise linear functions and then there was used a numerical method to calculate the transmission coefficient. Another method was applied in Ref. [10]. To determine the transmission probability and other parameters required to investigate the system they used the method of logarithmic derivate.

1.3 Tunneling through Triangular Barrier at Electron Field Emission

If we apply to a metal or semiconductor large electric field ($\sim 10^7$ V/cm) so that it is the cathode, then such a field pulls the electrons: it generates an electric current. This phenomenon is called electron field emission or "cold emission." Let us consider, for simplicity, the emission from the metal. We turn first to the picture of the motion of electrons in metal without an external electric field. To remove an electron from the metal, we need to do some work. Consequently, the potential energy of an electron in the metal is less than outside the metal. The simplest way this can be expressed is if we assume that the potential energy $U(x)$ inside the metal is equal to zero, while outside the metal it is equal to $U > 0$, so that the potential energy has the form shown in Figure 1.15. Simplifying in such manner the view of the potential energy, we actually operate with the average field in the metal. In fact, the potential inside the metal varies from point to point with a period equal to the lattice constant. Our approximation corresponds to the hypothesis of free electrons, since, as $U(x) = 0$ inside the metal there are no forces acting on an electron.

At such energy distribution of the electron gas the vast majority of electrons have the energy $E < U$ (at absolute zero temperature the electrons fill all the energy levels of $E = 0$ to $E = E_F < U$), where E_F is Fermi level. Let us denote the flow of electrons of the metal, falling from inside the metal on its surface, by J_0. Since the electrons have an energy $E < U$, then the flow is totally reflected by the jump in potential U, which takes place at the metal-vacuum interface (see Section 1.2.1).

The applied electric field F is directed toward the metal surface. Then the potential energy of an electron in the constant field of F, equal to qFx (electron charge equal to q) was added to

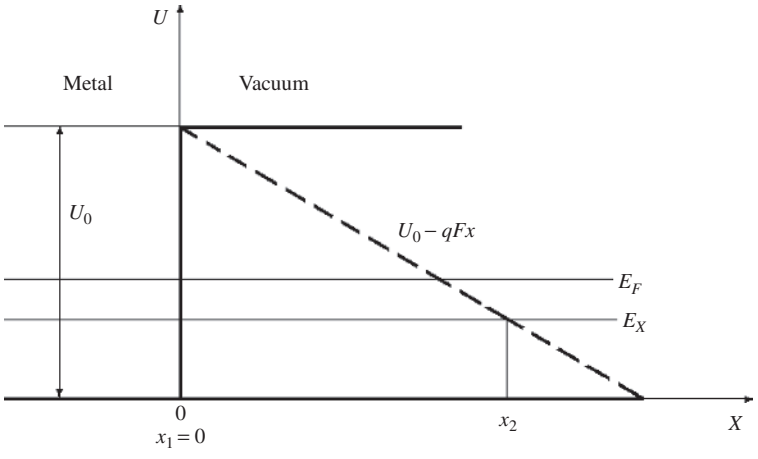

Figure 1.15 Band diagram of metal-vacuum interface without (solid line) and with (dashed line) applied electric field

the potential energy *U(x)* (Figure 1.15). Now the full potential energy will be

$$U^*(x) = U(x) - qFx = U_0 - qFx, (x > 0),$$
$$U^*(x) = 0, (x < 0). \tag{1.97}$$

Potential energy curve now has another view. It is shown in Figure 1.15 with dashed line. Note that large field cannot be created inside the metal, so the change of the *U(x)* takes place only outside the metal.

As it can be seen the triangular potential barrier is created. According to classical mechanics, an electron could pass through the barrier only if its energy is $E > U$. Such electrons are very little (they cause small thermionic emission). Therefore, according to classical mechanics the electron current is absent when the field is applied. However, if F is sufficiently large, the barrier is narrow, we have to deal with abrupt change of potential energy and classical mechanics is inapplicable: the electrons pass through the potential barrier.

Let us calculate the transmittance of the barrier for electrons with energy E_x moving along the *OX* axis. According to Equation (1.91) we have to calculate the integral

$$S = \int_{x_1}^{x_2} \sqrt{2m[U^*(x) - E_x]}dx, \tag{1.98}$$

where x_1 and x_2 are the coordinates of the turning points. The first turning point is (see Figure 1.15) obviously $x_1 = 0$, since for every energy $E_x < U$ the horizontal line E_x, representing the motion energy along *OX*, intersects the potential energy curve at $x = 0$. The second turning point is obtained, as can be seen from the figure, at

$$E_x = U_0 - qFx, \tag{1.99}$$

hence

$$x_2 = \frac{U_0 - E_x}{qF}, \tag{1.100}$$

consequently,

$$S = \int_0^{\frac{U_0 - E_x}{qF}} \sqrt{2m[U_0 - qFx - E_x]}dx. \tag{1.101}$$

Let us introduce the variable of integration

$$\xi = \frac{qF}{U_0 - E_x}x. \tag{1.102}$$

Then we get

$$S = \sqrt{2m}\frac{(U_0 - E_x)^{3/2}}{qF}\int_0^1 \sqrt{1-\xi}d\xi = \frac{2}{3}\sqrt{2m}\frac{(U_0 - E_x)^{3/2}}{qF} = \frac{2}{3}\sqrt{2m}\frac{(\Phi_0 - E_x)^{3/2}}{qF}. \tag{1.103}$$

Thus the transmission coefficient T for electrons with the energy of motion along the OX axis, equal to E_x, is

$$T(E_x) = T_0 e^{-\frac{4}{3}\frac{\sqrt{2m}}{\hbar}\frac{(\Phi_0 - E_x)^{3/2}}{qF}}. \tag{1.104}$$

This is the well-known Fowler–Nordheim equation [11].

The transmission coefficient is somewhat different for the different E_x, but as $E_x < U$, the average (in electrons energy) coefficient can be presented in the form

$$\overline{T} = \overline{T_0} e^{-\frac{F_0}{F}}, \tag{1.105}$$

where T_0 and F_0 are the constants depending on the type of the metal.

1.4 Effect of Trapped Charge in the Barrier

The influence of trapped charge on electron tunneling through the barrier has been intensively investigated in connection with the degradation of metal- oxide-semiconductor (MOS) structures with an ultra-thin oxide layer due to the carrier injection. The created charge in the oxide causes instability of MOS devices and oxide breakdown [12–15]. In the case where charges are trapped in the oxide with areal density Q_{ox} and centroid position X_b as referred to the cathode interface, the effective oxide electric field (F_{ox}) is no more equal to the cathode electric field (F)

$$F_{ox} = F + \frac{Q_{ox}}{\varepsilon_{ox}}\left(1 - \frac{X_b}{d_{ox}}\right). \tag{1.106}$$

where ε_{ox} is the oxide permittivity and d_{ox} is the oxide thickness.

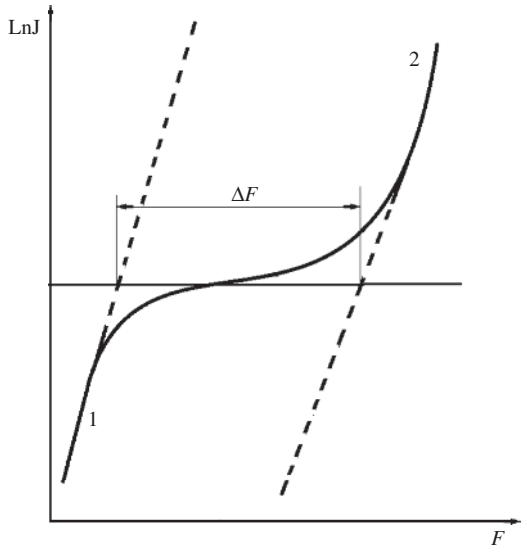

Figure 1.16 Schematic illustration of I-V curves shift due to charge trapping: (1) before charge trapping and (2) after charge trapping. Reproduced with permission from Ref. [16]. Copyright (1977), AIP Publishing LLC

Trapping of the charge will cause the shift of I-V characteristics (Figure 1.16).

Let's assume that negative charge (electrons) has been trapped. Trapping of the charge modifies the barrier shape significantly and as a result modifies the tunnel transparency (Figure 1.17) [13, 17–19]. To analyze the changing transmission probability and tunneling current changing due to charge we take into account that the trapped charge is localized at $x = X_b$ in the barrier (oxide) when $V_g < 0$ (Figure 1.17).

The transmission probability $T(E_x)$ for an electron at energy E_x is given by the following relationship [20]:

$$T(E_x) = T_0 \ \exp(-2 \int_{X=0}^{X_t} \sqrt{\frac{2m_{ox}}{\hbar^2}(U(x) - E_x)}dx), \tag{1.107}$$

where E_x is the perpendicular to the barrier electron energy (E) component, X_t is the tunnel distance in the oxide for the electron with energy (E_x), m_{ox} is the effective mass of the electron in oxide, $\hbar$ is the reduced Plank constant, q is the electron charge, and $U(x)$ is the potential barrier in oxide.

The Fowler–Nordheim (F–N) tunnel current density J_{FN}, which crosses the structure for given voltage V_g, is obtained by summing the contribution to the current of electrons at all energies E_x. The current density is given by the following expression [20]:

$$J_{FN} = \frac{4\pi q m_0}{\hbar^3} \int_{E_x} T(E_x)dE_x \int_{E_x}^{\infty} f(E,T)dE, \tag{1.108}$$

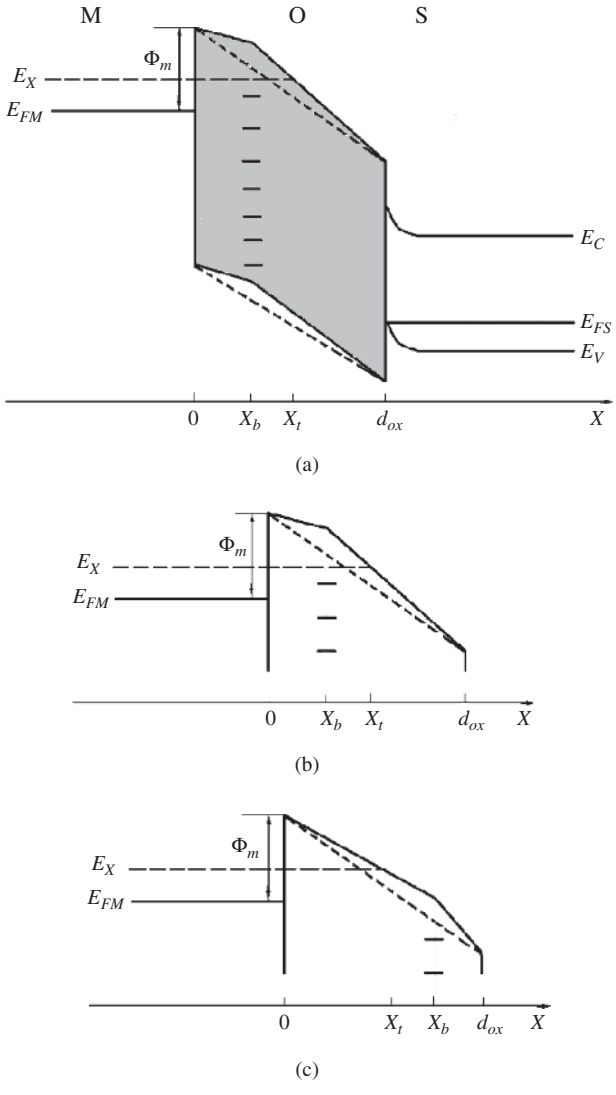

Figure 1.17 Energy band diagram of MOS structures (a) with (solid lines) and without (dashed lines) of the captured negative charge. Different location of trapped charge: (b) $X_b < X_t$ and (c) $X_b > X_t$

where m_0 is the mass of free electron and *f(E,T)* is the Fermi–Dirac distribution of electrons that depends on the temperature T [21, 22].

With respect to the trapped charges with density N_1 at $X = X_b$, there exist two fields for given voltage V_g in the oxide: one F_1 between the metal and X_b, the other F_2 between X_b and silicon [22]. Using the Gauss equation, one can determine the field E_1 as the function of the charge density N_1 and field F_2:

$$F_1 = \frac{qN_1}{\varepsilon_{ox}} + F_2. \tag{1.109}$$

The potential barrier $U(x)$ distribution can be obtained for given voltage V_g, by solving the Poisson equation:

$$U(x) = -\frac{q}{\varepsilon_0 \varepsilon_{ox}}(N_1 x) - qF_2 x + U(0). \text{ if } 0 \le x \le X_b, \tag{1.110}$$

$$U(x) = -\frac{q}{\varepsilon_0 \varepsilon_{ox}}(N_1 X_b) - qF_2 x + U(0). \text{ if } X_b \le x \le d_{ox}, \tag{1.111}$$

where ε_0 is the permittivity of vacuum, ε_{ox} is the relative permittivity of the oxide, $U(0)$ is the metal/oxide interface barrier (input barrier Φ_m), q is the absolute value of electron charge.

The expressions for tunneling probability and tunnel current depend on trapped charge location (X_b) in relation to length of tunneling path (X_t) (Figure 1.17). Taking into account Equations (1.109)–(1.111), the transmission probability $T(E_x)$ for an electron with energy E_x can be expressed, as a function of the electric fields F_1, by the expressions [17]:

1. if the charge centroid is localized in the tunnel distance X_t ($X_t > X_b$):

$$T(E_x) = T_0 \exp\left[-\frac{4}{3}\frac{(2m_{ox})^{1/2}}{\hbar q F_1} \times \left\{(\Phi_m - E_x)^{3/2} + \left(\frac{qN_1}{\varepsilon_{ox}F_1 - qN_1}\right)(\Phi_m - qF_1X_b - E_x)^{3/2}\right\}\right]; \tag{1.112}$$

2. if the charge centroid is localized outside the tunnel distance X_t ($X_t < X_b$):

$$T(E_x) = T_0 \exp\left[-\frac{4}{3}\frac{(2m_{ox})^{1/2}}{\hbar q F_1}(\Phi_m - E_x)^{3/2}\right]. \tag{1.113}$$

For the given voltage V_g, Equations (1.107)–(1.113) yield the potential barrier distribution in oxide, the transmission probability $T(E_x)$ and the current density J_{FN}.

In this case if the trapped charge is distributed on oxide thickness the shape of potential barrier is complicated significantly and calculation of transmission probability and tunnel current are more difficult.

The transient component of the current connected with charge trapping/detrapping processes can be observed [23]. It was shown that positive oxide charge assisted tunneling current also exhibits transient effect [24]. The transient behavior arises from the positive oxide charges, which help electron to tunnel through oxide, and they can escape to the Si substrate. As a result, the transient current should consist of three components in general, I_e, I_h, and I_t (Figure 1.18), if both positive and negative oxide charges are created [25].

I_e represents the negative oxide charge detrapping induced current, I_h is the positive oxide charge detrapping current, and I_t denotes the positive oxide charge assisted electron tunneling current. I_e and I_h have t^{-1} time dependence on the tunneling front model [23] while I_t has t^{-n} time dependence in the certain range of the measurement field. The power factor n is dependent on effective electron and hole tunneling barrier heights and tunneling carrier masses [24].

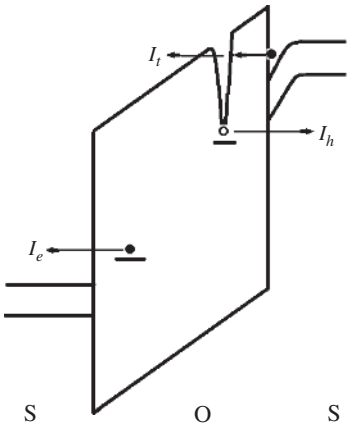

Figure 1.18 The schematic illustration of three transient components, I_e, I_h, and I_t. Reproduced with permission from Ref. [25]. Copyright (1999), AIP Publishing LLC

1.5 Transmission Probability in Resonant Tunneling Structures: Coherent Tunneling

At resonance tunneling the tunneling electron goes through double barriers via quantized states in the well [26]. Resonant tunneling of electrons represents sharp increase in the transmission coefficient of the quantum structure for the electrons which energy E coincides with the energy of one of the resonance levels E_n in the potential well. Despite the fact that at $E = E_n \ll U_1$, U_2 the transmission coefficients of the barriers T_1, $T_2 \ll 1$, the electron near the resonance "ignores" the barriers, passing through the entire structure without reflections. Resonant tunneling appears due to the interference of electron waves reflected from the barriers. As a result of interference at the resonance condition there are only the incident and transmitted boundary electron waves, and the reverse wave is completely extinguished. During this process the amplitude of the wave function inside the potential well is much greater than in the barriers. The mechanism of resonant tunneling from corpuscular positions can be represented as a delay of an electron inside the potential well on the time of its life τ_n (in the absence of scattering), during which the electron $\nu = \tau_n/L$ times encounter with barrier. Therefore, the probability of electron tunneling from the well increases in the ν times.

In resonant tunneling, the Schrodinger equation has to be solved simultaneously in three regions – emitter, well, and collector. Because of the quantized states within the well, the tunneling probability exhibits peak when the energy of the incoming particle coincides with one of the quantized levels. In the structure with barriers of finite thickness d_1 and d_2, the electron wave function is not located entirely within the well, but is smeared over the entire space. Nevertheless, there are selected values of energy, similar in magnitude to discrete resonant levels in completely isolated potential well, in which the amplitude of the wave function inside the well due to the interference of reflected from the barriers electron waves is much higher than the amplitude of the wave function outside the well. In this coherent-tunneling consideration, if the incoming energy does not coincide with any of the quantized levels, the global tunneling probably T_G is a product of the individual probability between the well and the emitter T_1, and

that between the well and the collector T_2,

$$T_{Gnr} = T_1 T_2. \tag{1.114}$$

However, when the incoming energy matches one of the quantized level, the wave function builds up within the well similar to a Fabry-Perot resonator, and the transmission probability becomes [7, 27].

$$T_{Gres} = \frac{4T_1 T_2}{(T_1 + T_2)^2}. \tag{1.115}$$

Applying the transfer matrix method, it is possible to calculate the transmission probability in resonant tunneling structures (RTSs) or double barrier resonant tunneling structures (DBRTSs). The potential energy diagram of such a structure in the general case with rectangular barriers is shown in Figure 1.19. The exact analytical solution is possible in this case.

According to our consideration in this case

$$\begin{pmatrix} A_1 \\ B_1 \end{pmatrix} = M_1 M_2 M_3 M_4 M_5 M_6 M_7 \begin{pmatrix} A_5 \\ B_5 \end{pmatrix}, \tag{1.116}$$

where M_1, M_5 are the input matrices Equation (1.95), M_2, M_6 are the barrier matrices Equation (1.94), M_3, M_7 are the output matrices Equation (1.96), and M_4 is well matrix Equation (1.93).

The final result can be presented as

$$T_G = \frac{T_1 T_2}{1 - 2\sqrt{R_1 R_2}\cos\theta + R_1 R_2}. \tag{1.117}$$

where T_1, T_2 are the transmission coefficient for first and second barriers; correspondingly, R_1, R_2 are the refractive coefficients for first and second barriers, respectively, and θ is the round-trip phase shift in the quantum well.

$$\theta = 2kw \tag{1.118}$$

where k is the wave vector in the well and w is the well width.

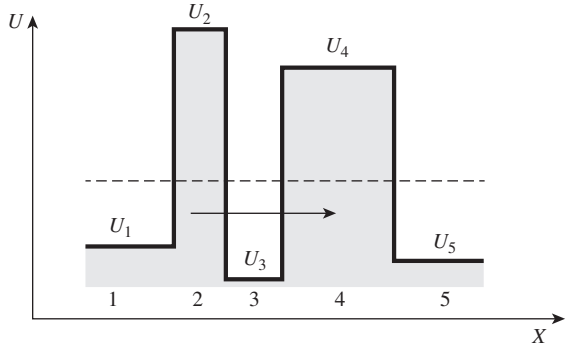

Figure 1.19 Potential-energy diagram of the double rectangular barrier case

As can be seen, the global transmission coefficient T_G through all structure is exactly derived.

We can rewrite Equation (1.117)

$$T_G = \frac{T_1 T_2}{(1 - \sqrt{R_1 R_2})^2 + 4\sqrt{R_1 R_2}\sin^2(\theta/2)}. \tag{1.119}$$

Here we use the trigonometric ratio

$$\cos\theta = 1 - 2\sin^2(\theta/2). \tag{1.120}$$

The condition of resonance is $\theta/2 = n\pi$ or $n\lambda = 2w$, where λ is the length of wave and n is the integer number.

At resonance $sin^2(\theta/2) = 0$ and we obtain the next equation for transmission coefficient

$$T_{Gres} = \frac{T_1 T_2}{(1 - \sqrt{R_1 R_2})^2}. \tag{1.121}$$

In real two barrier structures the transmission coefficients are small ($T \ll 1$). Then

$$\begin{aligned}(1 - \sqrt{R_1 R_2})^2 &= (1 - \sqrt{(1 - T_1)(1 - T_2)})^2 = (1 - \sqrt{(1 - T_1 - T_2 + T_1 T_2)})^2 \\ &= (1 - \sqrt{(1 - T_1 - T_2)})^2 = (1 - 1 + (T_1 - T_2)/2)^2 = \frac{(T_1 + T_2)^2}{4}.\end{aligned} \tag{1.122}$$

Here we used $T_1 T_2 = 0$ and Tailor series expansion

$$\sqrt{(1 - (T_1 + T_2))} = 1 - (T_1 + T_2)/2. \tag{1.123}$$

As a result in the case of resonant tunneling we have [7]

$$T_{Gres} = \frac{4T_1 T_2}{(T_1 + T_2)^2}. \tag{1.124}$$

The global transmission coefficient for double barrier resonance tunneling structure (Figure 1.19) can be put in the following general form [7, 28]:

$$T_G = \frac{C_0}{C_1 T_1 T_2 + C_2 \dfrac{T_1}{T_2} + C_3 \dfrac{T_2}{T_1} + C_4 \dfrac{1}{T_1 T_2}} \tag{1.125}$$

where T_1 and T_2 represent the transmission coefficients of the left and right barrier respectively which are exponentially dependent on energy. The C coefficients in Equation (1.125) are phase factors exhibiting much weaker energy dependence and, at first approximation, can

be used as constants if T coefficients are small ($T \ll 1$) ("strong localization" case). Under these conditions Equation (1.125) can be simplified, in the dominator the last term is dominated.

$$T_{Gnr} = \frac{C_0}{C_4} T_1 T_2 = T_1 T_2 \tag{1.126}$$

In this case then, the presence of potential energy well between two barriers has, in practice, little or no effect. The view of the transmission probability will be the same if the well is absent. The effect produced by the well is the reduction of the phase changing path of the total barrier.

For some special energy C_4 and C_1 go to zero. The main term is, consequently, canceled out and the resonance occurs. In this case, as easily seen from Equation (1.125), the global transmission coefficient T_{Gres} becomes

$$T_{Gres} = \frac{C_0}{C_2 \frac{T_1}{T_2} + C_3 \frac{T_2}{T_1}} = \frac{C_0 T_1 T_2}{C_2 T_1^2 + C_3 T_2^2} = \frac{T_1 T_2}{T_1^2 + T_2^2}. \tag{1.127}$$

Here we have assumed $C_0 = C_2 = C3 = 1$.

The more precise formula may be seen in Equation (1.115). For a symmetric structure, $T_1 = T_2$, and $T_{Gres} = 1$. Away from the resonance, the value T_G quickly drops by many orders of magnitude.

If $T_1 \gg T_2$ or $T_2 \gg T_1$ the relations (1.124) and (1.127) transform into

$$T_{Gres} = C \frac{T_{\min}}{T_{\max}} = \frac{T_{\min}}{T_{\max}}. \tag{1.128}$$

where T_{min} and T_{max} represent the smaller and larger among T_1 and T_2, respectively, while C is either C_0/C_2 or C_0/C_3 depending on whether or not $T_{max} = T_1$. In case of using as an initial formula (1.125) $C = 4$.

The comparison of Equations (1.126) and (1.128) show that resonance always implies an increased transmission coefficient since it is

$$\frac{T_{Gres}}{T_{Gnr}} = \frac{1}{T_{\max}^2}, \tag{1.129}$$

where T_{Gnr} represents the nonresonance (without resonance) value of T_G, that is, if no well has been presented between the two barriers.

Such an increase is, therefore, larger for smaller T_{max} and has vanished in the limiting case of $T_{max} \to 1$ (which, on the other hand, is incompatible with the assumption of strong localization). Equation (1.128) shows that regardless of how small T_1 and T_2 are, T_{Gres} can be order of unity under the only condition $T_1 = T_2$ while Equation (1.129) clearly indicates that the transmission coefficient can easily increase at the several orders of magnitude for arbitrary small changes in energy producing resonance.

Another important aspect of resonance concerns the wave function as schematically presented in Figure 1.20.

Without resonance the wave function $\Psi(x)$ monotonically and exponentially decreases within the classically forbidden regions thus reflecting the multiplication of the single barrier

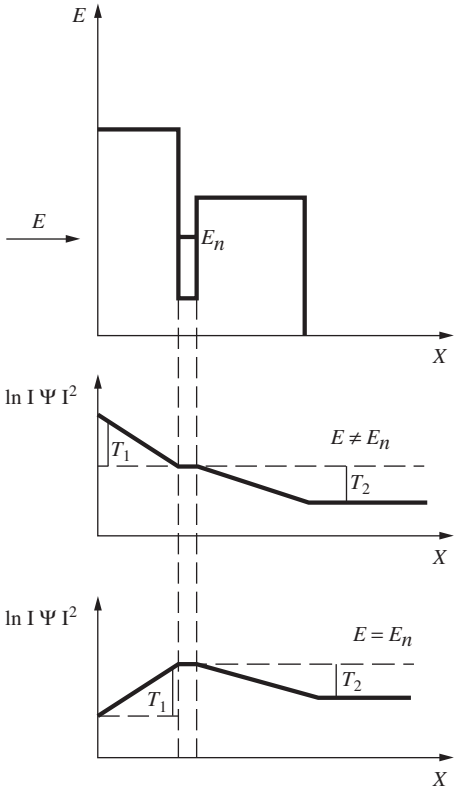

Figure 1.20 Schematic images of the wave function in the cases of resonance and without resonance. Reprinted with permission from Ref. [7]. Copyright (1984) by the American Physical Society

transmission coefficient (Equation (1.126)). At resonance, instead, the tunneling particle finds its eigenstate in the well where, consequently, the wave function has to be peaked with an exponential decrease on both sides (Figure 1.20). Since we have assumed both T_1 and $T_2 \ll 1$, this implies that the state is strongly localized. Because T_1 and T_2 are not zero, the localized states are, strictly speaking, quasi eigenstates with finite lifetime and energy width. The increase in transmission coefficient at resonance is a consequence of the wave function being peaked within the well. The typical dependence of transmission probability at tunneling through double-barrier resonant-tunneling structure is shown in Figure 1.21. The sharp resonance peaks are observed at $E = E_n$.

1.6 Lorentzian Approximation

Analysis shows that transmission coefficients through double barrier resonance tunneling structure are described by Equations (1.126) and (1.124) for nonresonant and resonant conditions, respectively. The sharp peak is observed at specific value of E_n. It allows performing above described approximations. For more precise description we have to use full

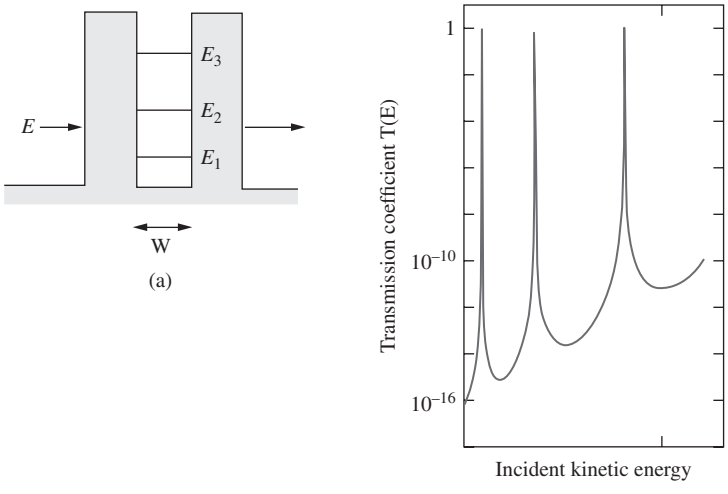

Figure 1.21 (a) Double barrier resonant tunneling structure. (b) Transmission coefficient of electron with energy E through a double barrier via coherent resonant tunneling. Transmission peaks occur when E aligns with E_n

Equation (1.117) and additionally analyze the influence of the wave function phase θ in well. We rewrite Equation (1.117), assuming R_1, $R_2 = 1$ [2]:

$$T_G = \frac{T_1 T_2}{1 - 2\sqrt{R_1 R_2}\cos\theta + R_1 R_2} = \frac{T_1 T_2}{(1 - \sqrt{R_1 R_2})^2 + 2\sqrt{R_1 R_2}(1 - \cos\theta)}$$
$$= \frac{T_1 T_2}{\left(\frac{T_1 + T_2}{2}\right)^2 + 2(1 - \cos\theta)}. \tag{1.130}$$

The sharpness of the resonance coefficient arises from the fact that R_1, $R_2 = 1$, T_1 and T_2 are very small, so that the denominator in Equation (1.130) is very small every time round-trip phase shift θ is close to the multiple of 2π.

At resonance $cos\theta = 1$ (see Equation (1.120)) we obtain Equation (1.124).

Close to resonance value we can expand the cosine function in Equation (1.130) in the Taylor series

$$(1 - \cos\theta) = \frac{1}{2}\theta^2 = \frac{1}{2}\left(\frac{d\theta}{dE}\right)^2 (E - E_n)^2 \tag{1.131}$$

and rewrite the transmission coefficient (Equation (1.130)) as

$$T_G = \frac{T_1 T_2}{\left[\frac{T_1 + T_2}{2}\right]^2 + \left(\frac{d\theta}{dE}\right)^2 (E - E_n)^2}. \tag{1.132}$$

Multiplying the denominator and numerator in Equation (1.132) on $(dE/d\theta)^2$ we obtain

$$T_G = \frac{\Gamma_1\Gamma_2}{\left[\frac{\Gamma_1+\Gamma_2}{2}\right]^2 + (E-E_n)^2}, \tag{1.133}$$

where

$$\Gamma_1 \equiv \frac{dE}{d\theta}T_1 \text{ and } \Gamma_2 \equiv \frac{dE}{d\theta}T_2. \tag{1.134}$$

This approximate result is often used (neglecting by energy dependence of Γ_1 and Γ_2) in place of the exact result (Equation (1.117)) for analytical calculations.

Multiply the denominator and numerator in Equation (1.133) on $(\Gamma_1+\Gamma_2)$ we have

$$T_G = \frac{\Gamma_1\Gamma_2(\Gamma_1+\Gamma_2)}{(\Gamma_1+\Gamma_2)\times\left[\left(E-E_n\right)^2+\left(\frac{\Gamma_1+\Gamma_2}{2}\right)^2\right]} = \frac{\Gamma_1\Gamma_2}{\Gamma_1+\Gamma_2}\times\frac{(\Gamma_1+\Gamma_2)}{(E-E_n)^2+\left(\frac{\Gamma_1+\Gamma_2}{2}\right)^2}$$

$$= \frac{\Gamma_1\Gamma_2}{\Gamma_1+\Gamma_2}\times\frac{\Gamma}{(E-E_n)^2+\left(\frac{\Gamma}{2}\right)^2} = \frac{\Gamma_1\Gamma_2}{\Gamma_1+\Gamma_2}\times A(E-E_n), \tag{1.135}$$

where $A(E-E_n)$ is a Lorentzian function:

$$A(E-E_n) = \frac{\Gamma}{(E-E_n)^2+\left(\frac{\Gamma}{2}\right)^2}, \tag{1.136}$$

where $\Gamma \equiv \Gamma_1+\Gamma_2$.

Total transmission function through n resonant energy levels can be presented as

$$T_T = \sum_n T_{Gn} = \frac{\Gamma_1\Gamma_2}{\Gamma_1+\Gamma_2}\sum_n A(E-E_n). \tag{1.137}$$

where n is the number of resonance level (Figure 1.21).

The magnitude of transmission is determined by the parallel combination of Γ_1 and Γ_2 while the width of the peak depends on the sum of Γ_2 and Γ_2.

The Lorentzian approximation for the transition function is often used for analytical calculations. It is reasonably accurate close to the resonance, but should not be used far from the resonance.

1.7 Time Parameters of Resonant Tunneling

In general, there are several time scales of importance in resonance tunneling structures: (1) the traversal time, the time needed to tunnel through a barrier; (2) the resonant state lifetime; and (3) the escape time [1]. All these factors influence the overall temporal response of the device.

A crucial aspect usually overlooked in experiments [29–35] is that, depending on initial conditions, nonnegligible time might be required before the high conductivity resonant state is fully established [7]. As a rule the analysis of resonant tunneling is based on the time-independent Schrodinger equation, which hence describes the stationary situation. This requires the carrier wave function at resonance to be strongly localized within the well. In this case it is possible to obtain Equation (1.117) for description of the resonance.

In resonant tunneling the main contribution to the characteristic time is from the well region of the device. In resonant tunneling, the electrons become trapped in a quasibound state and persist for some time before they "leak" out of the well through the second barrier. Resonant levels are metastable, that is, the average electron lifetime τ_{life} on them is finite. As a result, the resonant state lifetime can be appreciably larger than the barrier traversal time and the escape time. Therefore, we estimate the characteristic time by calculating the resonant state lifetime of the RTD (resonant tunneling diode).

The resonant state lifetime or, equivalently, the lifetime of the quasibound state can be estimated as follows. For simplicity it is assumed that the quantization direction is along the z axis. The velocity of the electron in this direction can be estimated as

$$v_z = \sqrt{\frac{2E_n}{m}}, \tag{1.138}$$

where E_n is the energy level of the quantized state. An attempt frequency can be defined as

$$f_{att} = \frac{v_z}{2L}, \tag{1.139}$$

where L is the effective one-way distance the electron travels in the well. Notice that the attempt frequency simply represents how often the electron encounters a boundary while reflecting back and forth within the well. The effective length L is given as

$$L = w + \frac{1}{k_{b1}} + \frac{1}{k_{b2}}, \tag{1.140}$$

where w is the width of the well and k_{b1} and k_{b2} are the imaginary wave vectors within the barriers. They represent the electron travel while partially penetrating the barriers. The probability per unit time of the electron escaping depends on the product of the attempt frequency (how often the electron encounters a boundary) and the transmissivity of each boundary, denoted as T_1 and T_2 (how likely it is for the electron to tunnel through the boundary). The lifetime is proportional to the inverse of the probability per unit time of the electron escaping from the quasibound level. The lifetime τ_{life} is then given as

$$\tau_{life} = \frac{1}{f_{att}(T_1 + T_2)}. \tag{1.141}$$

If it is further assumed that the electron can escape only from the second barrier, which is usually the case when the RTD is under high bias, then the lifetime becomes

$$\tau_{life} = \frac{1}{f_{att}T_2}. \tag{1.142}$$

The lifetime can also be estimated from the *uncertainty principle,* which states that

$$\Delta E \Delta t \geq \frac{\hbar}{2}. \tag{1.143}$$

Since the state is assumed to be quasibound, it has a finite lifetime. That lifetime is simply Δt. Therefore, the resonant lifetime is given as

$$\Delta t = \tau_{life} = \frac{\hbar}{2\Delta E}, \tag{1.144}$$

where ΔE is the half-maximum width of the transmission peak, $\Gamma_r/2$. Equating Equations (1.144) and (1.141) yields

$$\frac{\hbar}{2\Delta E} = \frac{1}{f_{att}(T_1 + T_2)}. \tag{1.145}$$

Using Equations (1.138)–(1.140), f_{att} can be written as

$$f_{att} = \frac{v_z}{2(w + 1/k_{b1} + 1/k_{b2})} = \frac{\sqrt{2E_n/m}}{2(w + 1/k_{b1} + 1/k_{b2})}. \tag{1.146}$$

Substituting Equation (1.146) into Equation (1.145) yields

$$\Gamma_r = 2\Delta E = \frac{\hbar\sqrt{2E_n/m}(T_1 + T_2)}{2(w + 1/k_{b1} + 1/k_{b2})}. \tag{1.147}$$

Therefore, the resonant lifetime is simply

$$\tau_{life} = \frac{2(w + 1/k_{b1} + 1/k_{b2})}{\sqrt{2E_n/m}(T_1 + T_2)}. \tag{1.148}$$

It is interesting to note that the resonant state lifetime describes both fully sequential and fully resonant conditions of good approximation. The resonant lifetime can be determined in somewhat different manner using a wavelike picture of the electron [1, 2].

Let's apply lifetime consideration to analysis of Γ_1 and Γ_2 parameters in Lorentzian approximation. One advantage of this approximation is that the entire physics is now characterized by just two parameters Γ_1 and Γ_2, which are defined in Equation (1.134). Physically Γ_1 and Γ_2 (divided by $\hbar$) represent the rate at which an electron placed between the barriers would leak out through the barriers into emitter, $\Gamma_1/\hbar$, and collector, $\Gamma_2/\hbar$, respectively.

It is possible to write the round-trip phase shift as $\theta = 2kL$ where L is effective width of the well (see Equation (1.140)) which includes also phase shifts associated with the reflections at the barriers.Then

$$\frac{dE}{d\theta} = \frac{1}{2L}\frac{dE}{dk} = \hbar f_{att}, \tag{1.149}$$

where $v \equiv dE/\hbar dk$ is the velocity with which an electron moves back and forth between the barriers. The quantity f_{att} means the number of times per second that the electron impinges on one of the barriers (that is, attempt to escape). It is equal to the inverse of the time that the electron takes to travel from one barrier to another and back.

The physical significance of Γ_1 and Γ_2 is easy to see. From Equations (1.134) and (1.149) we can write

$$\Gamma_1 \equiv \frac{dE}{d\theta}T_1 = \hbar f_{att}T_1 = \frac{\hbar\sqrt{2E_n/m}T_1}{2(w + 1/k_{b1} + 1/k_{b2})}, \tag{1.150}$$

$$\Gamma_2 \equiv \frac{dE}{d\theta}T_2 = \hbar f_{att}T_2 = \frac{\hbar\sqrt{2E_n/m}T_2}{2(w + 1/k_{b1} + 1/k_{b2})}, \tag{1.151}$$

$$\Gamma = \Gamma_1 + \Gamma_2 = 2\Delta E = \hbar f_{att}(T_1 + T_2) = \frac{\hbar\sqrt{2E_n/m}(T_1 + T_2)}{2(w + 1/k_{b1} + 1/k_{b2})}. \tag{1.152}$$

Fraction T_1 of the attempts on barrier 1 is successful while fraction T_2 of the attempts on barrier 2 are successful. Hence $\Gamma_1/\hbar$ and $\Gamma_2/\hbar$ tell us the number of times per second that an electron succeeds in escaping through barrier 1 and 2 respectively.

Finite lifetime of an electron at the resonance level causes broadening of the level (natural broadening), equal to

$$\Gamma_n = \frac{\hbar}{\tau_n}. \tag{1.153}$$

Electron lifetime and broadening are strongly dependent on the height and thickness of barriers and width of potential well, which determines the energy of the resonant level E_n, relative to the bottom of the well (Figure 1.22).

Various electron scattering processes that violate the coherence of electron waves within the layers and on the borders cause broadening of the resonance levels. This so-called collisional broadening of Γ_φ is associated with relaxation time τ_φ by relation similar to Equation (1.153):

$$\Gamma_\varphi \equiv \frac{\hbar}{\tau_\varphi}. \tag{1.154}$$

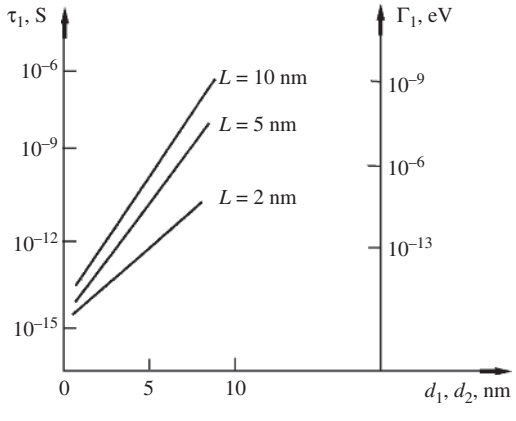

Figure 1.22 The lifetime τ_1 and natural width Γ_1 of low (the first) resonant level in quantum well on width L and barrier thicknesses d_1, d_2 dependences

Relaxation time τ_φ (see Equation (1.154)) decreases with increasing of impurities concentration, structural defects, and with increasing temperature. So, in pure gallium arsenide at room temperature $\tau_\varphi \sim 3 \times 10^{-13}$ s, and $\Gamma_\varphi \sim 2$ meV; at liquid nitrogen temperature (77 K) $\tau_\varphi \geq 10^{-11}$ s, and $\Gamma_\varphi \leq 0.10$ meV.

1.8 Transmission Probability at Electric Fields

From an experimental point of view it is very important to consider the double barrier resonance tunneling structure subjected to applied external electric fields (Figure 1.23). Under electric fields the potential barriers change their shape. And even the initial structure has the same potential barriers as the applied voltage destroys the symmetry of the barriers whose transmission coefficients are no longer equal. As can be seen, the shape of potential barriers has changed from rectangular to trapezoidal.

We use the transmission coefficient for one rectangular barrier to obtain the coefficient for trapezoidal barriers under an electric field. According to Equation (1.85) in the case of significantly thick and high barrier ($\alpha d \gg 1$):

$$T = \frac{1}{\left|M_{11}\right|^2} = \frac{16\alpha^2 k^2}{[-(\alpha - ik)^2 e^{+\alpha d}]^2} = \frac{16\alpha^2 k^2}{(\alpha - ik)^4} e^{-2\alpha d} = \frac{16\alpha^2 k^2}{(\alpha^2 + k^2)^2} e^{-2\alpha d} = T_0 e^{-2\alpha d} \quad (1.155)$$

The barrier changes its shape under an electric field

$$\alpha = \frac{1}{\hbar}[2m^*(U(x) - E)]^{1/2}. \quad (1.156)$$

Denote

$$U(x) - E = \Phi(x). \quad (1.157)$$

Under an electric field

$$\Phi = \Phi(x) = \Phi_0 - qFx. \quad (1.158)$$

We approximate the barrier by multistep function as some rectangular barriers with width *dx* and height *U(x)*. The transition coefficient for each element of barrier is

$$T^* = {T_0}^* e^{-2\alpha dx} \quad (1.159)$$

Then for all barrier

$$T = T_0 e^{\int_{x1}^{x2} -2\alpha dx} = T_0 e^{-\frac{2}{\hbar}\int_{x1}^{x2} [2m*(U(x)-E)]^{1/2} dx} = T_0 e^{-\frac{2}{\hbar}\int_{x1}^{x2} [2m*(\Phi_0 - qFx)]^{1/2} dx}, \quad (1.160)$$

where m^* is the constant (in barrier) and F is the electric field in the barrier.

In our case $x_1 = 0$; $x_2 = d$.

$$T = T_0 e^{-\frac{2}{\hbar}\int_{x1}^{x2} [2m*(\Phi_0 - qFx)]^{1/2} dx} = T_0 e^{-\frac{2}{\hbar}\sqrt{2m^*}\int_0^d (\Phi_0 - qFx)^{1/2} dx}. \quad (1.161)$$

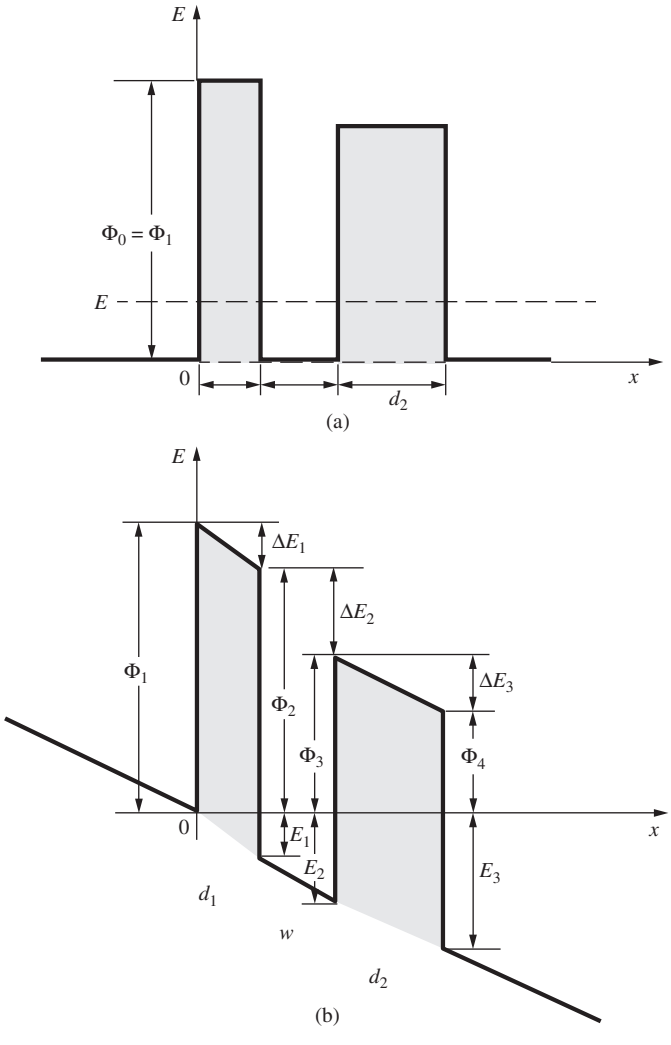

Figure 1.23 Double barrier structure without (a) and with (b) applied field

Take the integral in Equation (1.161)

$$\int_0^d [(\Phi_0 - qFx)]^{1/2} dx = \frac{\Phi_0^{3/2} - (\Phi_0 - qFd)^{3/2}}{3/2qF} \tag{1.162}$$

and we obtain the following equation for transmission probability of trapezoidal barrier.

$$T = T_0 \exp\left[-\frac{4}{3}\frac{\sqrt{2m^*}}{\hbar}\frac{\Phi_0^{3/2} - \left(\Phi_0 - qFd\right)^{3/2}}{qF}\right] \tag{1.163}$$

In the case of triangular barrier the second member in exponent of the function is equal to zero and we obtain a well-known Fowler–Nordheim equation [11].

$$T = T_0 \exp\left[-\frac{4}{3}\frac{\sqrt{2m^*}}{\hbar}\frac{\Phi_0^{3/2}}{qF}\right]. \tag{1.164}$$

As can be seen from Equation (1.163) Φ_0 is the height of barrier input and $(\Phi_0 - qFd)$ is the height of barrier output.

During the analysis of the transmission probability of two barrier resonance tunneling structure (Figure 1.23) we have to consider the transmission coefficients through the first (T_1) and the second (T_2) barriers. In this case the heights of barriers for coming electrons are significantly changed under electric field. It is necessary to take into account voltage dropping on each barrier and well. Based on Equation (1.163) we rewrite the transmission coefficients for the first and second barrier correspondingly

$$T_1 = T_{01} \exp\left[-\frac{4}{3}\frac{\sqrt{2m_1^*}}{\hbar}\frac{\Phi_1^{3/2} - {\Phi_2}^{3/2}}{qF_{b1}}\right], \tag{1.165}$$

$$T_2 = T_{02} \exp\left[-\frac{4}{3}\frac{\sqrt{2m_2^*}}{\hbar}\frac{\Phi_3^{3/2} - {\Phi_4}^{3/2}}{qF_{b2}}\right], \tag{1.166}$$

where Φ_1 is the first input barrier, Φ_2 is the first output barrier, Φ_3 is the second input barrier, and Φ_4 is the second output barrier.

They are expressed as:

$$\Phi_1 = \Phi_0 \tag{1.167}$$

$$\Phi_2 = \Phi_0 - qF_{b1}d_1 \tag{1.168}$$

$$\Phi_3 = \Phi_0 - qF_{b1}d_1 - qF_w w \tag{1.169}$$

$$\Phi_4 = \Phi_0 - qF_{b1}d_1 - qF_{b2}d_2 - qF_w w, \tag{1.170}$$

where F_{b1}, F_{b2}, and F_w represent the electric field in the barriers and well region, respectively, and they are

$$F_{b1} = V_a / \left(d_1 + \frac{\varepsilon_{b1}}{\varepsilon_{b2}}d_2 + \frac{\varepsilon_{b1}}{\varepsilon_w}w\right) \tag{1.171}$$

$$F_{b2} = V_a / \left(d_2 + \frac{\varepsilon_{b2}}{\varepsilon_{b1}}d_1 + \frac{\varepsilon_{b2}}{\varepsilon_w}w\right) \tag{1.172}$$

$$F_w = V_a / (w + \frac{\varepsilon_w}{\varepsilon_{b1}}d_1 + \frac{\varepsilon_w}{\varepsilon_{b2}}d_2. \tag{1.173}$$

Here ε_{b1}, ε_{b2}, and ε_w denote the dielectric constants of the barriers and well material while d_1, d_2, and w denote the barriers and well width, respectively, and V_a is the applied electric voltage.

Using Equations (1.165) and (1.166) it is possible to calculate the general transmission probability through two barrier resonance tunneling structure according to Equations (1.114), (1.115), or (1.135).

The dependence of the transmission coefficient, T_G, on applied electric field for resonance tunneling structure AlN-GaN-AlN calculated according to Equation (1.135) is shown in Figure 1.24. During the calculation of such parameters the double barrier resonance tunneling structure has been used: $d_1 = 2.5$ nm, $d_2 = 2.5$ nm, $w = 10$ nm, $\Phi_0 = \Phi_1 = \Phi_{GaN-AlN} = 2.0$ eV, $\varepsilon_{GaN} = 10.4\varepsilon_0$, $\varepsilon_{AlN} = 8.5\varepsilon_0$, $\varepsilon_0 = 8.85 \times 10^{-14}$ F/cm [34].

The analysis shows that even in the case of symmetrical structure with the same barriers the transmission coefficients of the first and second barriers are different. Using the nonsymmetrical structure with the left (first) barrier thinner, then the right (second) one, the condition for $T_1 = T_2$ might be recreated thus enhancing the resonance effects (see Equation (1.128)) looked for in experiments. But the possibility to realize the optimized condition (i.e., $T_G = 1$) is not guaranteed and even if this can be achieved, it would be true only for a particular resonance peak.

At high electric fields or in the case of some special structures, for example, at emission into vacuum (the second barrier is the vacuum) the shape of the second barrier is triangular (Figure 1.25).

In this case Equation (1.164) is applied for calculation of transmission probability through the second barrier.

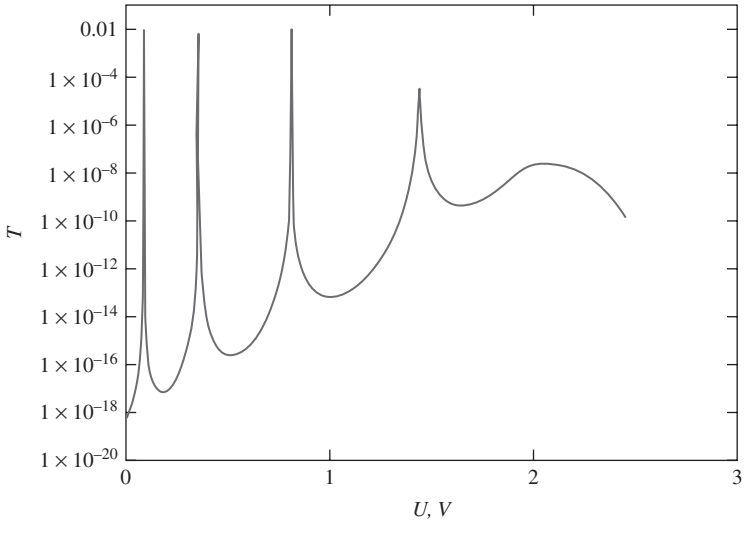

Figure 1.24 Calculated transmission coefficient for the AlN-GaN-AlN double barrier resonant tunneling structure

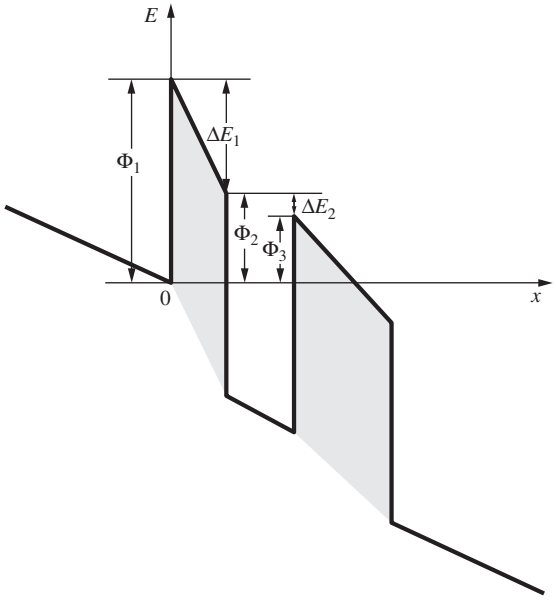

Figure 1.25 Two-barrier resonant tunneling structure under high electric field

1.9 Temperature Effects

1.9.1 One Barrier

Temperature dependence on transmission probability (Equation (1.117)) and tunnel current is caused by temperature induced carrier energy spreading. The Boltzmann distribution function and Fermi–Dirac distribution function, respectively, include the temperature

$$f(E) = \sqrt{\frac{E}{\pi k_B T}}\ \exp\left(-\frac{E}{k_B T}\right). \tag{1.174}$$

$$f(E) = 1/\{1 + \exp[(E - E_F)/k_B T]\}. \tag{1.175}$$

The F–N current density through the barrier (for example, SiO_2) can be calculated, as a function of temperature, under the assumption that the electrons in the emitting electrode (for example, Si) can be described by three-dimensional Fermi gas, according to classical approach while neglecting the Schottky effect as [11, 36]

$$J_{F-N}(T) = \frac{q m^*_{Si} k_B T}{2\pi^2 \hbar^3} \int_0^{\Phi} \ln\left[1 + \exp\left(\frac{E_F(T) - E}{k_B T}\right)\right] \times \exp\left(-\frac{4\sqrt{2m^*_{ox}}(\Phi - E)^{3/2}}{3\hbar q F}\right) dE, \tag{1.176}$$

where q is the absolute electron charge, m^*_{Si} and m^*_{ox} are the effective electron mass into the Si and SiO_2, respectively, $k_B T$ is the thermal energy, $\hbar$ is the reduced Planck constant, F is the electric field across the insulator, and E_F is the Fermi level.

In the low-temperature approximation the conventional temperature independent F–N analytical expression can be derived from relation (1.176) in the form [36]

$$J^0_{F-N} = AF^2 \exp\left(-\frac{B}{F}\right), \tag{1.177}$$

where A and B are the so-called pre-exponential and exponential F–N coefficients defined as

$$A = \frac{q^3 m^*_{Si}}{16\pi^2 \hbar m^*_{ox} \Phi}, \tag{1.178}$$

$$B = \frac{4\sqrt{2m^*_{ox}}\Phi^{3/2}}{3\hbar q}. \tag{1.179}$$

Although relation (1.177) has been derived under low-temperature approximation, it can be used to empirically describe the temperature dependence of the F–N current in MOS structure after extraction of the effective coefficients *A(T)* and *B(T)* [37].

As a rule the next analytical but approximate formula that has been proposed to account for the variation with temperature of the F–N emission current are used [20, 38]

$$J_{F-N}(T) = \frac{\pi c k_B T}{\sin(\pi c k_B T)} J^0_{F-N}, \tag{1.180}$$

where $c = 2\sqrt{2m_{ox}\Phi}/q\hbar F$.

This analytical approximation is not applicable at high temperatures and/or low electric field such that $ck_BT \geq 1$.

In order to overcome this limitation in Ref. [37] the new series expansion (Sommerfeld expansion) of the F–N current versus temperature derived in Equation (1.176) has been obtained

$$\frac{J_{F-N}(T)}{J_{F-N}(0)} = 1 + \frac{\pi^2}{6} T(E_F)(k_B T)^2 + \frac{7\pi^2}{360} T^{//}(E_F)(k_B T)^4 + \ldots + C_{2n} T^{(2n-2)}(E_F)(k_B T)^{2n} + \ldots. \tag{1.181}$$

The advantage of the given analytical formula is that (1) it does not diverge for any critical condition as it is in the case for relation (1.180), and (2) the desired accuracy of the analytical expression can be controlled by the polynomial order up to which the expansion is done. Figure 1.26 illustrates the capability of the proposed in Ref. [37] analytical expression (1.181) expanded to the sixth order and that of relation (1.180) to approximate the exact F–N current Equation (1.174). In this example, the maximum error given by relation (1.181) does not exceed 15% for 400 °C, whereas it is larger than a factor 2 for relation (1.180).

The experimental results on F–N tunneling [37] confirm (1) the strong impact of temperature on the F–N current amplitude, especially for temperatures above 250 °C; and (2) the good linearity of the F–N plots whatever the temperature is. The last point demonstrate that the low temperature analytical model of relation (1.180) can still be applied up to 400 °C, but with the temperature-dependent effective pre-exponential and exponential F–N coefficients *A(T)* and *B(T)*.

At electron injection from degenerated silicon into oxide the good agreement of experimental and calculated results has been achieved after the assumption on linear variation of Φ with

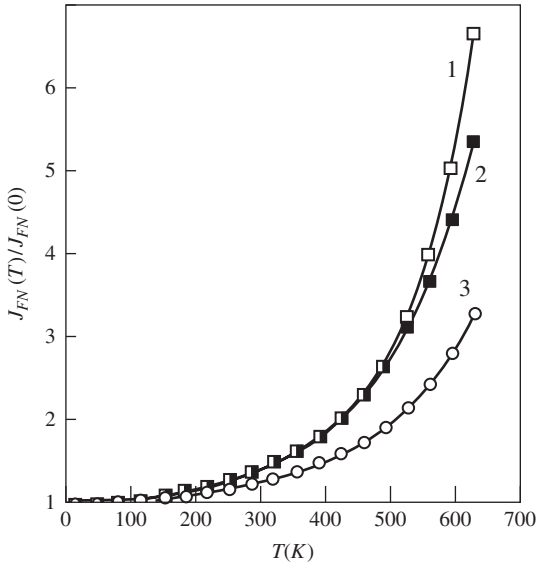

Figure 1.26 Theoretical relative variations of the F–N currents as obtained using the exact formula and analytical approximations: (1) exact dependence, (2) analytical approximation according to formula (1.181), and (3) analytical approximation according to formula (1.180). Reproduced with permission from Ref. [37]. Copyright (1995), AIP Publishing LLC

temperature with $d\Phi/dT = -2.4 \times 10^{-4}$ eV/°C, but at emission from metal electrode $d\Phi/dT = -2.67 \times 10^{-4}$ eV/°C [20, 39, 40]. It is well established that temperature induces decrease in the barrier height at the Si/SiO_2 interface [41]. As the tunneling probability exponentially depends on Φ this effect is large enough. For a given temperature, the decrease of 0.1 eV of Φ leads to nearly one decade of increase in J_{FN} for $F = 8$ MV/cm. The theoretical F–N coefficients A and B have been extracted for different temperatures. They are in good agreement with the experimental ones. This clearly demonstrates that the temperature behavior of the F–N tunnel current can be reasonably well interpreted by the classical model of relation (1.176), which accounts satisfactorily for the temperature-induced carrier energy statistical spreading. It is worth noting that the effective barrier height is always found to be smaller than the "actual" barrier height deduced from the relation, which takes into account the Fermi level variation with temperature over the whole temperature range [37]:

$$E_F(T) = E_{F0}\left[1 - \frac{\pi^2}{12}\left(\frac{k_B T}{E_{F0}}\right)^2\right], \tag{1.182}$$

where $E_{F0} = \hbar^2(3\pi^2 N_s)^{2/3}/(2m^*_{Si})$.

This result clearly indicates that all the approaches based on only low-temperature F–N approximation Equation (1.177) cannot explain the behavior with temperature of the F–N emission by including only the temperature dependence through Fermi level variation.

It is now clear that the temperature-induced carrier energy distribution accounted for 3D model is the dominant mechanism for the F–N current changing with temperature. The strong effect of temperature experimentally observed [37, 42, 43] is rather due to the temperature effect on the barrier height caused by carrier energy distribution.

1.9.2 Double-Barrier Resonance Tunneling Structure

The temperature can effect the resonance time. The key point is that the thermal motion of the atoms in any sample contributes in making the potential energy time dependent. As far as this effect is concerned, from a qualitative point of view different cases can be distinguished. If the variations of potential energy E_p are very small or/and very slow (compare to τ_0), then E_p can be considered not to depend on time to all practical purposes. If, instead, E_p significantly varies in values on a time scale comparable or smaller than τ_0, then a more complicated analysis is required.

Overall it is expected that the temperature will give rise to broadening of the resonance peaks and decrease in their effects on the current measured in experiments.

It is very important to consider the effect due to the electron thermal population [7]. The important conclusion is reached that at resonance a variety of current-versus-T relationship can result depending on the relative position of the resonance state and the Fermi energy (E_F). In particular, currents increasing as well as decreasing with T and complicated nonmonotonic temperature behavior are possible. Each state gives rise to its own (individual) J vs. T dependence according to its energy position. In real samples where many such states are presented, different (individual) current behavior is to be expected at each resonant peak. This is in agreement with experiments showing that the conductance at peak is proportional to $exp[(T_0/T)^{1/2}]$ where T_0 is individual for the considered peak [44].

As the temperature varies the cathode carrier concentration at the resonant energy also varies and so does the current J measured in experiments. At the same time the carrier thermal velocity also increases with T and, with semiconductor or metal cathode, this implies an increase in the electron flux hitting the barrier, hence J. This latter is, however, only a minor effect (because the thermal velocity depends on $T^{1/2}$) with respect to that mentioned earlier whose temperature dependence comes from the exponential factor in the Fermi distribution function.

Because we essentially deal with the carrier concentration within the definite narrow energy window (the width of the resonant eigenstate centered on E_n) the effects to be expected depend on its position relative to E_n. If E_n and E_F are close (compared with k_BT), an increase of T spreading out the distribution function can only lead to decrease of particle concentration at the resonance energy, hence to decrease of tunneling current. In this case J exhibits a metallic type of behavior.

In any case, for large increase of temperature a subsequent increase in current may occur since, as the distribution function spreads out, the carrier concentration can become nonnegligible at other, higher eigenstates whose contribution will rapidly become important. If, on the other hand, the distance between E_n and E_F is large, an increase of current is first expected to occur as a consequence of the increase in carrier concentration available for resonant tunneling. Here too, however, a subsequent metallic type of behavior can arise for the same reasons as given above [7].

References

1. K.F. Brennan and A.S. Brown. *Theory of Modern Electronic Semiconductor Devices* (New York, John Wiley & Sons, Inc., 2002).
2. S. Datta. *Electronic Transport in Mesoscopic Syst.ems*, Ed. H. Ahmed, M. Pepper, A. Broers (Cambridge, Cambridge University Press, 1995), pp. 247–75.
3. M. Ya. Azbel, Eigenstates and properties of random systems in one dimension at zero temperature, *Physical Review B* **28**, 4106 (1983).
4. A.F. Kravchenko and V.N. Ovsyuk. *Electron Processes in Solid-State Low-Dimensional System* (Novosibirsk University Press, 2000), 448p (in Russian).
5. S.N. Lykov, V.G. Gasumyantz, and S.A. Rykov. *Quantum Mechanics, Part 2*, (St Petersburg, St Petersburg State Technical University, 2004) (in Russian).
6. O.V. Tretyak and V.Z. Lozovskyy. *Foundation of Semiconductor Physics* Vol. 2 (Kyiv University Press, 2009) (in Ukrainian).
7. B. Ricco and M.Ya. Azbel, Physics of resonant tunneling. The one-dimensional double-barrier case, *Physical Review B* **29**, 1970 (1984).
8. Y. Ando and T. Itoh, Calculation of transmission tunneling current across arbitrary potential barriers *Journal of Applied Physics* **61**, 1497 (1987).
9. W.W. Liu and M. Fukuma, Exact solution of the Schrodinger equation across an arbitrary one-dimensional piecewise-linear potential barrier, *Journal of Applied Physics* **60**, 1555 (1986).
10. A.F.M. Anwar and M.M. Jahan, Resonant tunneling devices. *Encyclopedia of Nanoscience and Nanotechnology*. Ed. H.S. Nalwa (American Scientific Publisher, Vol. 9, pp. 357–70, 2004).
11. R.H. Fowler and L. Nordheim, Electron emission in intense electric fields, *Proceedings of the Royal Society of London Series A* **119**, 173 (1928).
12. P. Bellutti and N. Zorzi, High electric field induced positive charges in thin gate oxide, *Solid-State Electronics* **45**, 1333 (2001).
13. I.C. Chen, S.E. Holland and C. Hu, Electrical breakdown in thin gate and tunneling oxides, *IEEE Transactions on Electron Devices* **32**, 413 (1985).
14. Y. Hokari, Stress voltage polarity dependence of thermally grown thin gate oxide wearout, *IEEE Transactions on Electron Devices* **35**, 1299 (1988).
15. P. Samanta and C.K. Sarkar, Analysis of positive charge trapping in silicon dioxide of MOS capacitors during Fowler-Nordheim stress, *Solid-State Electronics* **32**, 507 (1989).
16. P. Solomon, High-field electron trapping in SiO_2, *Journal of Applied Physics* **48**, 3843 (1977).
17. S.J. Oh and Y.T. Yeow, Voltage shifts of Fowler-Nordheim tunneling J-V plots in thin gate oxide MOS structures due to trapped charges, *Solid-State Electronics* **32**, 507 (1989).
18. J. Lopez-Villanueva, J. Jimenez-Tejada, P. Cartujo, J. *et al*. Analysis of the effects of constant-current Fowler–Nordheim-tunneling injection with charge trapping inside the potential barrier, *Journal of Applied Physics* **70**, 3712 (1991).
19. P.S. Ku and D.K. Schroder, Charges trapped throughout the oxide and their impact on the Fowler-Nordheim current in MOS device, *IEEE Transactions on Electron Devices* **41**, 1669 (1994).
20. M. Lenzlinger and E.H. Snow, Fowler-Nordheim tunneling into thermally grown SiO_2, *Journal of Applied Physics* **40**, 278 (1969).
21. S.M. Sze. *Physics of Semiconductor Devices* (John Wiley & Sons, Inc., Hoboken, NJ 1981).
22. A. Aziz, K. Kassmi, Ka Kassmi, and F. Olivie, Modelling of the influence of charges trapped in the oxide on the $I(V_g)$ characteristics of metal-ultra-thin oxide-semiconductor structures, *Semiconductor Science and Technology* **19**, 877 (2004).
23. D.J. Dumin and J.R. Maddux, Correlation of stress-induced leakage current in thin oxides with trap generation inside the oxides, *IEEE Transactions on Electron Devices* **40**, 986 (1993).
24. T. Wang, N.K. Zous, J.L. Lai, and C. Huang, Hot hole stress induced leakage current (SILC) transient in tunnel oxides, *IEEE Electron Device Letters* **19**, 411 (1998).
25. N.K. Zous, T. Wang, C.-C. Yeh, and C.W. Tsai, Transient effects of positive oxide charge on stress-induced leakage current in tunnel oxides, *Applied Physics Letters* **75**, 734 (1999).
26. S. Luryi and A. Zaslavsky, Quantum-effect and hot-electron devices, in S.M. Sze, Ed, *Modern Semiconductor Device Physics* (John Wiley & Sons, Inc, New York, 1998), pp. 253–341.
27. S.M. Sze and K.K. Ng. *Physics of Semiconductor Devices*, 3rd edn (John Wiley & Sons, Inc., New York 2007).

28. O. Kane. *Tunneling Phenomena in Solids*, ed. E. Burnstein and D. Lundquist (Plenum, New York, 1969), pp. 79–92.
29. L.L. Chang, L. Esaki, and R. Tsu, Resonant tunneling in semiconductor double barriers, *Applied Physics Letters* **24**, 593 (1974).
30. M. Hirose, M. Morita, and Y. Osaka, Resonant tunneling through Si/SiO_2 double barriers, *Japanese Journal of Applied Physics* **16**, 561 (1977).
31. T.C.L.G. Sollner, W.D. Goodhue, P.E. Tannenwald, C.D. Parker, and D.D. Peck, Resonant tunneling through quantum wells at frequencies up to 2.5 THz, *Applied Physics Letters* **43**, 588 (1983).
32. M. Buttiker and R. Landauer, Traversal time for tunneling, *Physical Review Letters* **49**, 1739 (1982).
33. M. Buttiker, Larmor precession and the traversal time for tunneling, *Physical Review B* **27**, 6178 (1983).
34. Yilmazoglu, O., Considine, L., Joshi, R. *et al*. (2011) Resonant electron-emission from a flat surface AlN/GaN system with carbon nanotube gate electrode. In *Technical Digest of International Vacuum Nanoelectronics Conference*, Wuppertal, Germany, July 18–22, 2011, pp. 216–217.
35. B. Ricco, M.Ya. Azbel, and M.N. Brodsky, Novel mechanism for tunneling and breakdown of thin SiO_2 films, *Physical Review Letters* **51**, 1795 (1983).
36. J.J. O'Dwyer, *The Theory of Electrical Conduction and Breakdown in Solids Dielectrics*, (Clarendon, Oxford, 1973).
37. G. Pananakakis, G. Ghibaudo, and R. Kies, Temperature dependence of the Fowler–Nordheim current in metal-oxide-degenerate semiconductor structures, *Journal of Applied Physics* **78**, 2635 (1995).
38. R.H. Good and W. Muller, *Field emission, Hanbuch der Physik*, Vol. 21 (Springer, Berlin, 1956).
39. M.O. Aboelfotoh, Schottky-barrier behavior of a Ti-W alloy on Si(100), *Journal of Applied Physics* **61**, 2558 (1987).
40. K.S. Kim and M.E. Lines, Temperature dependence of chromatic dispersion in dispersion-shifted fibers: Experiment and analysis, *Journal of Applied Physics* **73**, 2069 (1993).
41. A. Hadjiadji, G. Salace, and C. Petit, Fowler–Nordheim conduction in polysilicon (n^+)-oxide–silicon (p) structures: Limit of the classical treatment in the barrier height determination, *Journal of Applied Physics* **89**, 7994 (2001).
42. G. Salace, A. Hadjiadji, C. Petit, and M. Jourdain, Temperature dependence of the electron affinity difference between Si and SiO_2 in polysilicon (n^+)–oxide–silicon (p) structures: Effect of the oxide thickness, *Journal of Applied Physics* **85**, 7768 (1999).
43. G. Salace, A. Hadjiadji, C. Petit, and Dj. Ziane, The image force effect on the barrier height in MOS structures: correlation of the corrected barrier height with temperature and the oxide thickness, *Microelectronics Reliability* **40**, 763 (2000).
44. A.B. Fowler, A. Hartstein, and R.A. Webb, Conductance in restricted-dimensionality accumulation layers, *Physical Review Letters* **48**, 196 (1982).